國 立 交 通 大 學

電 信 工 程 學 系 碩 士 班

碩 士 論 文

傳播對室外多輸入多輸出系統容量影響之研究

Propagation Effects on Outdoor MIMO Capacity

研究生：蔡明哲

指導教授：唐震寰 博士

中華民國九十三年七月

I

傳播對室外多輸入多輸出系統容量影響之研究

Propagation Effects on Outdoor MIMO Capacity

研 究 生：蔡明哲　　　　　　　　Student : Ming-Zhe Tsai

指導教授：唐震寰　　　　　　　　Advisor : Dr. Jenn-Hwan Tarng

國 立 交 通 大 學

電 信 工 程 學 系 碩 士 班

碩 士 論 文

A Thesis

Submitted to Department of Communication

College of Engineering

National Chiao Tung University

in Partial Fulfillment of the Requirements

for the Degree of

Master of Science

in

Communication Engineering

July 2004

Hsinchu, Taiwan, Republic of China

中 華 民 國 九 十 三 年 七 月

傳播對室外多輸入多輸出系統容量影響之研究

研究生：蔡明哲　　　　　指導教授：唐震寰 博士

國立交通大學

電信工程學系碩士班

摘要

多輸入多輸出系統的技術概念發射端與接收端信號的結合處理獲得高速率通道傳輸容量。該系統於多路徑環境下可利用路徑的低相關性達到相當高的通道容量。本論文採用頻域向量通道響應系統模擬四對四的多輸入多輸出系統，於台灣國立交通大學校園內對主波導性、阻擋波導性及非波導性環境進行通道響應實地量測並計算其通道容量。對於通道容量而言，吾人發現於傳播環境中，天線間距、傳輸接收端的距離、區域散射波以及頻寬都有很大的影響。然而陣列擺向在非波導性環境下有顯著的影響，主波導性則是影響較小。對於相關特性而言，相關特性跟周遭環境有很大的關連。量測環境越複雜，由多重路徑信號造成的入射角度擴展均方根越大與通道容量呈現正相關的現象。我們並結合一實體統計空-時通道模型與量測結果評估通道容量，一如預期通道容量與量測傳輸距離、區域散射波及天線間距有關係。

Propagation Effects on Outdoor MIMO Capacity

Student：Ming‐Zhe Tsai   Advisor：Dr. Jenn‐Hwan Tarng

Department of Communication Engineering

National Chiao Tung University

Abstract

Large capacity is obtained via the potential decorrelation among MIMO spatial radio channels.   A fully correlated MIMO radio channel only offers one equivalent subchannel for transmission and a completely decorrelated MIMO spatial radio channel potentially offer multiple subchannels depending on the antenna array arrangement and propagation effects. In this paper, effects of propagation conditions such as LOS, OLOS and NLOS, propagation distance, local scatterer distributions, signal bandwidth and antenna array element spacing on 4x4 MIMO capacity are investigated through extensive measurement in macrocellular environments. It is found that the rms AOA (Angle-of-Arrival) and number of multipath components (MCPS) are the two fundamental parameters to affects the capacity. Environments under rich scattering signals such as NLOS condition and existing of local scatterers exhibiting a high rms angular spread of AOA ensures a high probability of achieving independent fading and hence boosts capacity. The increase of the array element spacing decreases the correlation among spatial channels, i.e., increasing the capacity. It is also found that the increase of signal bandwidth will increase the signal resolution and hence number of MPCs increases, which enhances the capacity. It seems that the capacity is independent of propagation distance and angular spread of AOD.

誌謝

首先，我要對我的指導教授唐震寰老師致上最誠摯的感謝，感謝老師在我碩士兩年的研究生涯中，給于我最細心與凡心的指導與叮嚀，並帶領我一窺無線通訊領域研究的奧妙。

其次，對於波散射與傳播實驗室的學長與同學們也要致上我深深的謝意，他們所給予我在知識上和精神上的啟示與鼓勵以及在實驗量測中的協助，對完成本篇論文有莫大的助益。

最後，要感謝的是我最親愛的父母親、怡婷由於他們給予我的支持與關懷，使我在人生的過程裡得到最細心的呵護與照顧，讓我在成長與求學的過程中能夠有所依靠。

僅以此篇論文獻給所有關心我的人。

<div align="right">

蔡明哲

國立交通大學，新竹市

中華民國九十三年七月

</div>

Contents

List of Figures

List of Tables

Chapter 1

Introduction

The explosive growths of the wireless industry and the internet are creating a huge market opportunity for wireless data access. Limited internet access at low speeds (a few tens of kilo-bits per second at most) is already available as an enhancement to some second-generation (2G) cellular systems. However those systems were originally designed with the sole purpose of providing voice services and at most short messaging, but not high-speed data transfers. To increase system capacity of mobile networks of 3G and B3G communication systems, smart antennas have utilized SDMA (Space Division Multiple Access) technique to increase signal gain and to reduce interference. Multiple-input-multiple-output (MIMO) system, which has multiple antenna elements at both the transmitter and receiver, is illustrated in Fig. 1. The idea behind MIMO is that the signals on the transmit antennas and that of the receive antennas are "combined" [1] in such a way that the quality (bit error rate) or the data rate (bit/sec) of the communication will be improved. Such an advantage can be used to increase both the network's quality and the operator's revenues significantly. A core idea in MIMO systems is space-time signal processing in which time dimension (the natural dimension of digital communication data) is complemented with the spatial dimension inherent in the use of multiple spatially distributed antennas.

Since MIMO systems can be viewed as an extension of the so-called "smart

antennas", a popular technology using antenna arrays for improving wireless transmission dating back several decades. Conventional smart antenna systems yield a capacity enhancement or range extension over conventional fixed beam antenna installations by focusing their beam patterns towards an addressed volume associated with the signaling space of the desired traffic channel.

Fig. 1 MIMO system configuration

Large capacity is obtained via the potential decorrelation in the MIMO radio channel within the confine of the limited radio spectrum allocated to these systems, which can be exploited to create many parallel subchannels. However, the potential capacity gain is highly dependent on the multipath richness in the radio channel, since a fully correlated MIMO channel only offers one subchannel, while a completely decorrelated channel offers multiple subchannels depending on the antenna configuration-the most striking property of MIMO systems is the ability to turn multipath propagation, usually a pitfall of wireless transmission, into an advantage for increasing the user's data rate. [2]

The practical realization of the potentially huge capacities will depend on various

factors, none more than propagation and antenna arrangement. Measurement of outdoor MIMO channels have been reported in [3] without providing insights into the relation between the channel structure, the corresponding capacity and the propagation. The influence of spatial fading correlation at either transmit or the receive side of a wireless MIMO radio link has been addressed in [4]. While the models used in [4] are simple and allow gaining insight into the impact propagation conditions on MIMO capacity they assume that only spatial fading correlation is responsible for the rank structure of the MIMO channel. In practice, however, the realization of high MIMO capacity in actual radio channels is sensitive not only to the fading correlation but also to the structure of scattering in the propagation [5]. Ref [6] provides an approach modeling MIMO channel to investigate the impact of MIMO capacity on more realistic channel and several key questions regarding outdoor MIMO channels, including (1) What is the capacity of a typical outdoor MIMO channel? (2) What are the key propagation parameters governing the capacity behavior? (3) Under what conditions do we get a high rank MIMO channel (and hence high capacity)? (4) What is a simple analytical model describing the capacity behavior of outdoor MIMO wireless channels accurately? Environment under rich scattering signals exhibiting a high azimuth spread ensures a high probability of achieving independent fading and hence boosts capacity. Measurements of MIMO channels are therefore necessary in order to characterize the performance of these systems in real environments.

In this paper, we analyze the factors of impact on capacity for different sites and try to find the answers to the above questions. We use a physical-statistical spatio-temporal channel model, which consists of a site-specific deterministic model with a geometrically based single bounce statistical model.

The paper is organized as following: In chapter 2, the fundamental theory of MIMO system will be introduced and the governing condition of obtaining high capacity is introduced. In Chapter 3, measurement campaign is described and channel multipath parameters such as AOA, AOD and frequency response extracted from measurement data. In chapter 4, the impact of propagation and antenna arrangement on capacity are analyzed.   In chapter 5, the conclusion is presented

Chapter 2

Capacity Estimation of MIMO Systems

Today's inspiration for research and applications of wireless MIMO systems was triggered by the initial Shannon capacity results obtained independently by Bell Lab's researchers E. Telatar and J. Foschini, further demonstrating the seminal role of information theory in telecommunications. The analysis of theoretical capacity gives information on how the channel model or the antenna setup itself may influence the transmission rate. It helps the system designer benchmark transmitter and receiver algorithm performance. Here we examine the capacity aspects of MIMO systems compared with single input single output (SISO) and single input multiple output (SIMO) and multiple input single output (MISO) systems.

2.1 Capacity Formulas

A. Shannon capacity of wireless channels

Given a single channel corrupted by an additive white Gaussian noise (AWGN), at a level of SNR denoted by ρ, the capacity (rate that can be achieved with no constraint on code or signaling complexity) can be written as

$$C_{SISO} = \log_2(1+\rho) \text{ bps/Hz} \tag{1}$$

This can be interpreted either by an increase of 3dB in SNR required for each extra bit per second per Hertz or by requiring roughly a doubling of transmitter

power to obtain double capacity (To go from 1bps/Hz to 11bps/Hz，the transmitter power must be increased by 1000 times). In practice wireless channels are time-varying and subject to random fading. In this case we denote h the unit-power complex Gaussian amplitude of the channel at the instant of observation. The capacity, written as：

$$C_{SISO} = \log_2(1 + \rho|h|^2) \text{ bps/Hz} \tag{2}$$

becomes a random quantity, whose distribution can be computed. The cumulative distribution of this "1x1" case (one antenna on transmit and one on receive) is shown on the left in Fig.2-1 We notice that the capacity takes, at times, very small values, due to fading events.

B. Multiple antennas at one end

Given a set of M antennas at the receiver (SIMO system), the channel is now composed of M distinct coefficients $h = [h_0; h_1; \cdots; h_{M-1}]$ where h_i is the channel amplitude from the transmitter to the i-th receiver antenna. The expression for the random capacity can be generalized to

$$C_{SIMO} = \log_2(I_M + \rho h_{Mx1} h_{Mx1}^H) \tag{3}$$

where $[\cdot]^H$ represents Hermitian transposition, can be approximated as

$$C_{SIMO} = \log_2(1 + M\rho) \quad \text{bps/Hz} \tag{4}$$

M is the number of the receiver. Compared to the capacity of SISO system

$$C_{SISO} = \log_2(1 + \rho) \quad \text{bps/Hz}$$

It shows that slow logarithmic growth of the bandwidth efficiency limit.

In Fig. 2-1, we see the impact of multiple antennas on the capacity distribution with 4 and 10 antennas respectively. This is due to the spatial diversity, which reduces fading and the higher SNR of the combined antennas.

However going from 4 to 10 antennas does not give very significant improvement as spatial diversity benefits quickly level off.   The increase in average capacity due to SNR improvement is also limited because the SNR is increasing inside the log function in (3).   We also show that the results obtained in the case of multiple transmit antennas and one receive antenna, "4x1" and "10x1" when the transmitter does not know the channel in advance.   In such circumstances the multiple transmit antennas cannot beamform blindly.   Conventional multiple antenna systems are good at improving the outage capacity performance, attributable to the spatial diversity effect but this effect saturates with the number of antennas.

C. Capacity of MIMO links

We now consider a full MIMO link as Fig. 1 with N transmit antennas and M receive antennas respectively.   The channel is represented by a matrix of size M x N with random elements denoted by H_{MxN}, we have the now famous capacity equation [1]

$$C_{MIMO} = \log_2(I_M + \frac{\rho}{N}HH^H) \ bps/Hz \tag{5}$$

when $\frac{1}{N}HH^H \approx I_N$, (5) can be approximated as

$$C_{MIMO} \approx k \cdot \log_2(1+\rho) \ bps/Hz \qquad k = \min\{M,N\} \tag{6}$$

boosting compared to SISO channels and fast growth compared to SIMO channels
    Foschini [1] and Telatar [3] both demonstrated that the capacity in (5) grows linearly with k=min (M, N) rather than logarithmically.   This result can be intuited as follows：the determinant operator yields a product of min(M,N) nonzero eigenvalues of its (channel-dependent) matrix argument, each eigenvalue characterizing the SNR over a so-called channel eigenmode.   An eigenmode corresponds to the transmission

using a pair of right and left singular vectors of the channel matrix as transmit and receive antenna weights, respectively. Thanks to the properties of the log, the overall capacity is the sum of capacities of each of these modes, hence the effect of capacity multiplication. Clearly, this growth is dependent on properties of the eigenvalues. If they decayed away rapidly then linear growth would not occur. However, the eigenvalues have a known limiting distribution and tend to be spaced out along the range of this distribution. Hence, it is unlikely that most eigenvalues are very small and the linear growth is indeed achieved. In theory and in the case of idealized random channels, limitless capacities can be realized provide that we can afford the cost and space of many antennas and RF chains. In reality the performance will be dictated by the practical transmission algorithms selected and by the physical channel characteristics.

Applying MIMO techniques to wireless communication to meet the anticipated demand for high bit rate, real time services within limited bandwidths. MIMO propagation channel asymptotically gives M x N diversity and min (M, N) orthogonal communication channels for fully uncorrelated antennas. A large number of parallel channels is attractive since they are capable of carrying parallel information in the same bandwidth. The eigenvalue decomposition deduced from the propagation channel matrix (M x N) is an important parameter in this context because it determines the effective number of available parallel subchannels. Next we will introduce the concept of eigen-analysis on MIMO channel, a matrix solution leads itself to an analytical approach where the eigenvalues of the transmission system lead to a definition of the maximum gain as the largest eigenvalue.
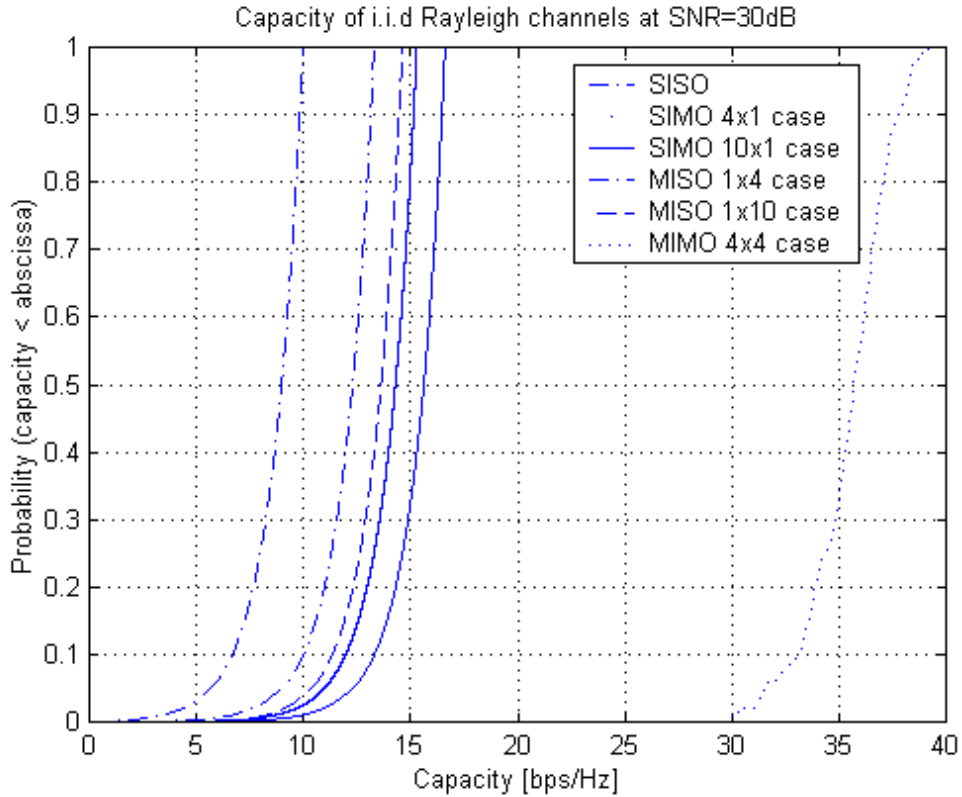
Fig. 2-1 Shannon capacity as function of number of transmitter and receiver antennas

2.2 Spatial Correlation Coefficient

The complex correlation coefficient is a complex number that is less than unity in absolute value. Let a, b be two complex random variables, the complex correlation coefficient of a and b is defined as

$$< a,b >= \frac{E[ab^*] - E[a]E[b^*]}{\sqrt{\left(E\left[|a|^2 - |E[a]|^2 \right] \right)\left(E|b|^2 - |E[b]|^2 \right)}}$$

where * denotes the complex conjugate operation. It is assumed that all antenna elements in the two arrays have the same polarization and the same radiation pattern. The spatial complex correlation coefficient at the BS between antenna m_1 and m_2 is given by

$$\rho_{m_1 m_2}^{BS} = < h_{m_1 n}, h_{m_2 n} > \tag{7}$$

where $< a, b>$ computes the correlation coefficient between a and b. The spatial complex correlation coefficient observed at the MS is similarly defined as
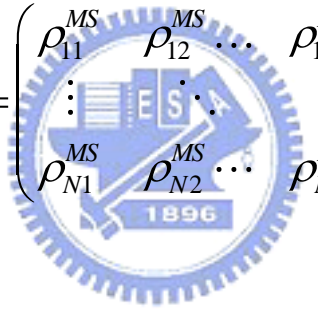
$$\rho_{m_1 m_2}^{MS} =< h_{mn_1}, h_{mn_2} >$$ (8)

Given (7) and (8), we can define the following symmetrical complex correlation Matrices

$$R_{BS} = \begin{pmatrix} \rho_{11}^{BS} & \rho_{12}^{BS} \cdots & \rho_{1M}^{BS} \\ \vdots & \ddots & \vdots \\ \rho_{M1}^{BS} & \rho_{M2}^{BS} \cdots & \rho_{MM}^{BS} \end{pmatrix}_{M \times M}$$

and

$$R_{MS} = \begin{pmatrix} \rho_{11}^{MS} & \rho_{12}^{MS} \cdots & \rho_{1N}^{MS} \\ \vdots & \ddots & \vdots \\ \rho_{N1}^{MS} & \rho_{N2}^{MS} \cdots & \rho_{NN}^{MS} \end{pmatrix}_{N \times N}$$

$$\rho^{BS} = \frac{1}{M(M-1)} \left(\sum_{\substack{i=1, j=1 \\ i \neq j}}^{M} \left| \rho_{m_i m_j}^{BS} \right| \right)$$ (9)
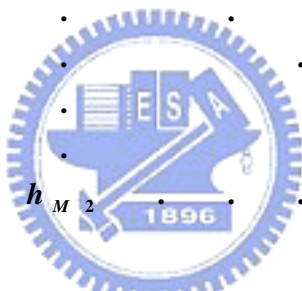
$$\rho^{MS} = \frac{1}{N(N-1)} \left(\sum_{\substack{i=1, j=1 \\ i \neq j}}^{N} \left| \rho_{n_i n_j}^{MS} \right| \right)$$ (10)

2.3 Eigenanalysis on MIMO channel

A way to estimate the number of independent channels between two terminals in a rich scattering environment is to use the eigenvalue decomposition of the instantaneous correlation matrix **R** defined as

$$R=HH^H$$

where **H** is the narrowband complex channel matrix and $[\cdot]^H$ represents Hermitian transposition. **H** is expressed as

$$
H\ (\ f\ )\ =\
\begin{bmatrix}
h_{11} & h_{12} & \cdot & \cdot & \cdot & \cdot & \cdot & h_{1N} \\
h_{21} & h_{22} & \cdot & \cdot & \cdot & \cdot & \cdot & h_{2N} \\
\cdot & \cdot & \cdot & & & & & \cdot \\
\cdot & \cdot & & \cdot & & & & \cdot \\
\cdot & \cdot & & & \cdot & & & \cdot \\
\cdot & \cdot & & & & \cdot & & \cdot \\
\cdot & \cdot & & & & & \cdot & \cdot \\
h_{M1} & h_{M2} & \cdot & \cdot & \cdot & \cdot & \cdot & h_{MN}
\end{bmatrix}
$$

where h_{mn} is the complex channel coefficient between the m-th antenna at the receiver and the n-th antenna at the transmitter. Note that each element of the channel matrix **H** is a function of frequency. Then (5) becomes

$$C(f) = \log_2(\det(I_M + \frac{\rho}{N}H(f)H(f)^H))$$

For the frequency-selective case, the capacity needs to average over the frequencies:

$$C_{MIMO,avg} = \frac{1}{B}\int_B \log_2(\det(I_M + \frac{\rho}{N}H(f)H(f)^H))df$$

where **B** is the bandwidth. Note that the channel matrix **H** is normalized such that

$$E<|h_{mn}|^2>=1$$

From [7], in order to get the weight vector associated to the eigenvalue decomposition, it is convenient to use the singular value decomposition (SVD) of a matrix **H** defined as

$$H = U \Sigma V^H \tag{11}$$

where

$$\Sigma = diag(\sigma_1, \cdots, \sigma_p)$$

σ_i are real, nonnegative singular values.

$$U = [u_1 \ u_2 \cdots \ u_m] \in C^{m \times n}$$
$$V = [v_1 \ v_2 \cdots \ v_n] \in C^{m \times n}$$

where **U** and **V** are unitary matrices and **u** and **v** are the left and right singular vectors, respectively. σ is called the singular values of **H.** There is an important relationship between the SVD of H and the eigenvalue decomposition (EVD) of R such that $\sigma = \sqrt{\lambda}$ where λ is the eigenvalue. A channel matrix H_{MxN} offers k=min {M, N} parallel channels with different mean gains and correlated fast fading statistics. These k channels are accessible by applying the appropriate weight vectors **u** and **v** at both the transmitter and receiver antenna array. Then (11) is just a compact way of writing the set of independent channels

$$HV_1 = \sqrt{\lambda_1} U_1$$
$$HV_2 = \sqrt{\lambda_2} U_2$$
$$.$$
$$.$$
$$.$$
$$HV_n = \sqrt{\lambda_n} U_n$$

The SVD is particularly useful for interpretation in the antenna context. If one estimates the response of each antenna element to a desired transmitted signal, one can optimally combine the elements with weights selected as a function of each

element response. For instance, choosing one particular eigenvalue, it is noted that V_i is the transmit weight factor for excitation of the singular value $\sqrt{\lambda_i}$. A receive weight factor of U_i^*, a conjugate match, gives the receive voltage S_r and the square of that the received power

$$S_r = U_i^* U_i \sqrt{\lambda_i} = \sqrt{\lambda_i}$$
$$P_r = |S_r|^2 = \lambda_i$$

This clearly shows that the matrix of transmission coefficients may be diagonalized leading to a number of independent orthogonal modes of excitation, where the power gains of the i-th mode or channel is λ_i. The weights applied to the arrays are given directly from the columns of the **U** and **V** matrices. Thus, the eigenvalues and their distributions are important properties of the arrays and the medium, and the maximum gain is given by the maximum eigenvalue. The number of nonzero eigenvalues may be shown to be the minimum value of M and N. The situation is illustrated in Fig. 2-2, where the total power is distributed among the N parallel channels by weight factors α. An important parameter is the trace of HH^H, i.e., the sum of the eigenvalues

$$Trace = \sum_i \lambda_i$$

which may be shown to have a mean value of MN.
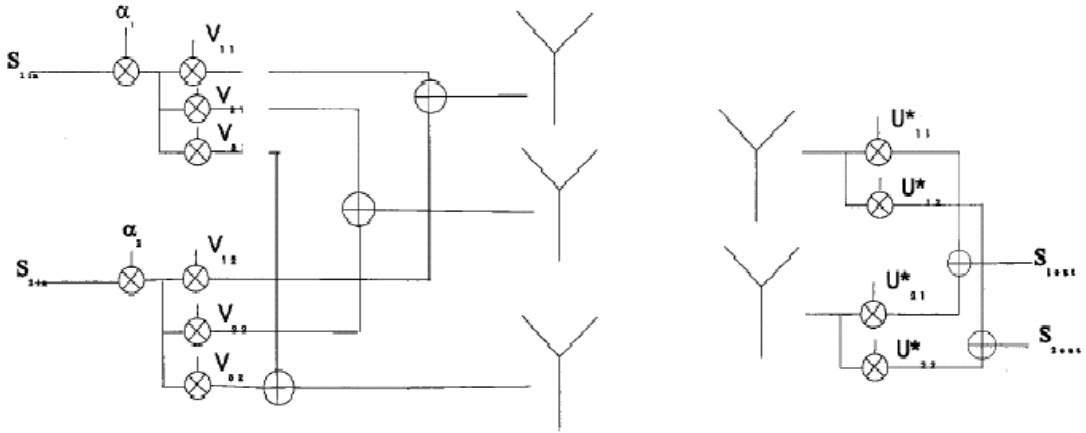
Fig. 2-2 Transmission from three (N) transmit antennas to two (M) receive antennas.   There are two independent channels (the minimum of M and N), which are excited by the **V** vectors on the transmit side and weighted by the **U** vectors on the receive side.   The power is divided between the two channels according to the "water filling" principle.   This is a maximum capacity excitation of the medium.   In case only maximum array gain is wanted, only the maximum eigenvalue is chosen (one channel)

Once the channel matrix **H** is diagonalized by SVD and obtain the power gain in the k-th channel is given by the k-th eigenvalue i.e., the signal to noise ratio (SNR) for the k-th channel equals

$$\gamma_k = p_k \frac{\lambda_k}{\sigma_n^2}$$

where p_k is the power assigned to the k-th channel, λ_k is the k-th eigenvalue and σ_n^2 is the noise power.   The number of independent eigenmode channels λ_k depends on the number resolvable paths L and the number of antenna elements at the transmitter and the receiver. According to Shannon the maximum capacity of k parallel channels equals

$$C = \sum_k \log_2(1 + \gamma_k)$$

$$C = \sum_k \log_2(1 + \lambda_k \frac{p_k}{\sigma_n^2})$$

where the mean SNR is defined as

$$\rho = \frac{E\{\sum_k p_k \lambda_k\}}{\sigma_n^2}$$

Assuming all noise powers to be the same.   Given the set of eigenvalues $\{\lambda_k\}$, the input power p_k are determined to maximize the capacity by using Gallager's "water filling" theorem [8] i.e.,

$$\frac{1}{\lambda_1} + p_1 = \cdots = \frac{1}{\lambda_k} + p_k = D$$

where each channel is filled up to a common level D. Thus the channel with the highest gain, i.e., eigenvalue, receives the largest share of the power. The constraint on the powers is that

$$\sum_k p_k = P = Cons\tan t$$

The weight factors α_k in Fig. 2-2 equal $\frac{p_k}{P}$.   In case the level D drops below a certain $\frac{1}{\lambda_k}$ then that power is set to zero, i.e., that λ_k eigenmode channel diminishes.
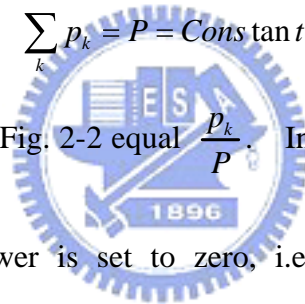
2.4 MIMO LOS Channels

In this section, we provide condition guaranteeing a high rank MIMO channel in real environment. We suggest that rank properties are governed by simple geometrical propagation parameters.

Considering the N transmitter, M receiver setup described in Fig. 2-3, only uniform linear arrays (ULA) are considered in this paper, but the analysis can be extended to other array topologies, like uniform circular arrays. We assume bore-sight propagation from the transmit array to the receive array. In addition, we assume the signal radiated by the k-th transmit antenna to impinge as a plane wave on the receive array at an angle of θ_k. This assumption is justified when the antenna aperture is much smaller than the range R and the receive antenna array is within the far-field of the transmit antenna array. The propagation of a plane wave representing path k impinging on the antenna array causes a time delay $\Delta_{r,k}^{Rx}$ at different antenna elements. This small time delay of the arrival of the wavefronts between different antennas results in a phase-shift $\phi_{r,k}^{Rx}$ at these receive antennas. The delay $\Delta_{r,k}^{Rx}$ at receive antenna r compared to the first antenna is defined as:

$$\Delta_{r,k}^{Rx} = \frac{(r-1)\cdot d_r \sin\phi_k^{Rx}}{c}$$

The array propagation vector h_k^{Rx} contains these phase shifts with respect to the first antenna for a certain path k. Denoting the signature vector induced by the k-th transmit antenna as $h_k^{Rx} = [1 \quad e^{-j\frac{2\pi d_r}{\lambda}\sin(\theta_k)} \quad \cdots \quad e^{-j\frac{2\pi(M-1)d_r}{\lambda}\sin(\theta_k)}]^T$, where d_r and d_t are the receive and transmit antenna spacing, respectively, we have $H = [h_1^{Rx} \quad h_2^{Rx} \quad \cdots h_N^{Rx}]$. The array propagation vector defines the spatial response of an antenna array. The common phase shift due to the distance R between transmitter

and receiver has no impact on capacity and is therefore ignored.   Clearly, when the θ_k (k=1,2…N) (all other parameters being fixed) approach zero we find that **H** approaches the all ones matrices and therefore has rank 1.   In practice, this happens for large R.   As the range decrease, linear independence between the signature starts to build up.   Since the capacity of a MIMO channel depends on the actual channel coefficients, which are random variables, the capacity is a random variable as well. A communication system suffers only if the capacity is lower than needed for a transmission therefore usually the outage capacity is given.   The 1% outage capacity defines the minimum capacity that is ensured over 99% of the transmission time.

Hence we choose to use the full orthogonality between the signatures of adjacent pairs of transmit antennas as a criterion for the

receiver to be able to separate the transmit signatures well hence implying high capacity.   This condition [6] reads

$$< h_k, h_{k+1} > = \sum_{m=0}^{M-1} e^{j\frac{2\pi d_r m}{\lambda}[\sin(\theta_{k+1})-\sin(\theta_k)]} = 0 \qquad (12)$$

For practical values of R, d_r and d_t, orthogonality will occur for small θ_k.   We can therefore set $\sin\theta_k \approx \frac{(k-1)d_t}{R}$ (k=1,2…K).   Consequently, condition (12) can be written as

$$\sum_{m=0}^{M-1} e^{j2\pi m\frac{d_t d_r}{\lambda R}} = 0$$

which implies

$$\frac{d_t d_r}{R} \geq \frac{\lambda}{M}. \qquad (13)$$

Note that this is not sufficient to achieve exact orthogonality, although for a large number of receive antenna it will tend to be sufficient.   In practice, for larger values of antenna spacing, the transmit antennas can fall into the grating lobes of the receive array in which case orthgonality is not realized. (13) can be written into

$$\frac{\lambda}{Md_r} \leq \frac{d_t}{R}$$

which can be interpreted in terms of basic antenna theory as follows: The angular resolution of the receive array (inversely proportional to the aperture in wavelengths) should be less than the angular separation between two neighboring transmitter. Of course a similar condition in terms of transmit resolution can be by enforcing orthogonality between the rows of **H.** In a pure LOS situation orthogonality can only be achieved for very small values of range R. For example at a frequency of 2.44GHz with M=4, a maximum of R=15m is acceptable for 1m transmit antenna spacing (i.e.10λ).
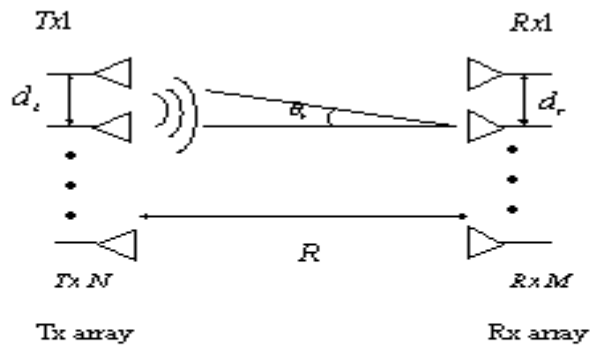

Fig 2-3 N-input M-output configuration

Fig. 2-3 N-input M-output configuration

Chapter 3

Measurement campaign and set-up

As described in the introduction, a vast measurement campaign was planned to investigate the MIMO channel in real environments. Published literatures [9] so far has most relied on assumptions about the statistical behavior of this wireless channel. Although this has proven the concept and allowed further investigations to be undertaken, rigorous MIMO channel measurement campaign conducted is therefore necessary in order to characterize the performance of these systems in real environments. The objective of this chapter is therefore to describe the measurement set-up, the measurement campaign and extract the parameters from measurement raw data.

3.1 Measurement Set-up

For measurement of the time-varying and directional mobile radio channels, the RUSK vector channel sounder was employed [9]. The measurement equipment and its system diagram and are shown in Fig 3-1 and Fig 3-2. The sounder system consists of a mobile transmitter (Tx) that is omni-directional, and a fixed receiver (Rx) with an 8-element array antenna, each having a beamwidth of 120^0. A fast multiplexing system switches between each of these elements in turn in order to take a complete vector snapshot of the channel in $12t_p$. Periodic multi-frequency excitation with 120MHz bandwidth is used, i.e., the time resolution is 8.3ns. The

Doppler bandwidth of up to 20kHz allows complete statistical analysis of the time varying radio channel with respect to different azimuthally directions of the impinging waves. In the case of a remote link measurement, Tx/Rx synchronization is maintained by two rubidium references. This calibration process of rubidium reference removes the tracking error of the measurement system and as a result of phase and delay normalization. Allowing the system a warm-up time about 60 minutes to stabilize oscillator and amplifier minimizes temporal drift of the measurement system. The telemetry allows remote control of the digital receiving unit (DRU) from portable transmitting station (PTS) location.

The channel impulse responses of the antenna array are recorded as "vector snapshots" in rapid succession. After receiving by Rx, signals are gathered to DRU and sent to a personal computer (PC) to analyze where AOA is estimated by using Unitary ESPRIT with sub-array smoothing technology. An overview about array signal processing including estimation of the AOA and a comparison of ESPRIT with other algorithm can be found in [10]. The receiving antenna was mounted on a rooftop at 2.44 GHz with the transmission power of 1w. The transmitter antenna was carried in a trolley and was 1.8 meter above the road. In order to get multipath components, we sampled data by moving measurements along selected routes with walking speed. We performed the measurements at the time of 10:00~20:00 with many pedestrians and vehicles, which may result in random scattering effects.
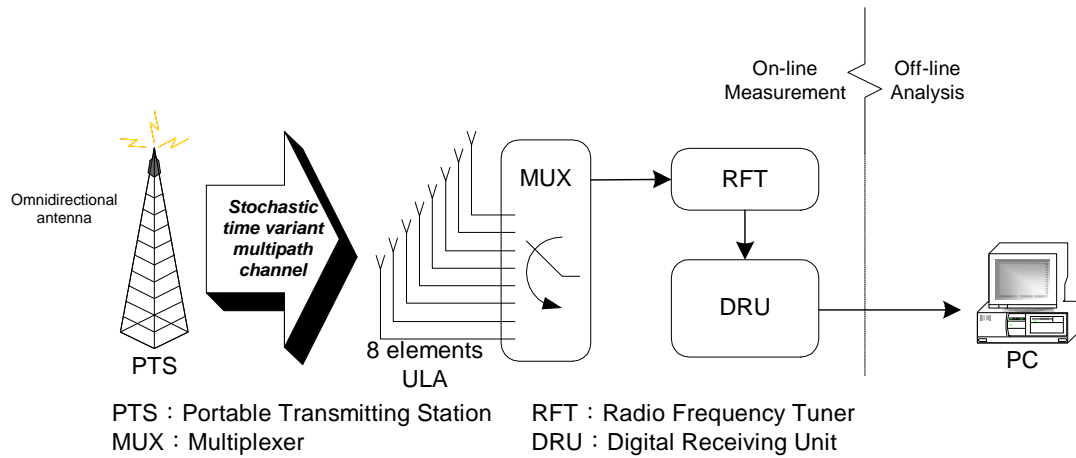
Fig. 3-1 System diagram of the RUSK vector channel sounder

(a)   (b)

Fig. 3-2 RUSK vector channel sounder. (a) Transmitting unit. (b) Receiving unit.

3.2 Measurement Campaign

There are four measurement sites illustrated in Fig. 3-3. Detailed experimental

setup or arrangement at each site is given as follows:

Measurement sites：National Chiao Tung University Guang Fu campus

Site 1 along route no.1 with total route length: 50m (12700

snapshots）

Site 2 along route no.2 with total route length: 170m (36700

snapshots)

Site 3 along route no.3 with total route length: 200m (4200

snapshots,)

Site4 along route no.4 with total route length: 250m (4800

snapshots)

Moving speed：

route no.1 and route no.2 : Speed=2~3 km/hr

route no.3 and route no.4 : Speed=10 km/hr

Tx-Rx distance：route no.1：15~50m

route no.2：140m~150m

route no.3：193~203m

route no.4：250~259m
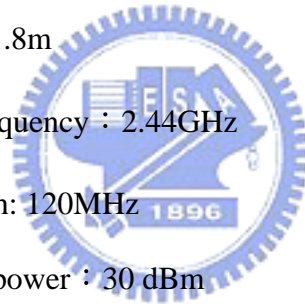
Transmit antenna：Omni-directional

Height：1.8m

Center frequency：2.44GHz

Bandwidth: 120MHz

Transmit power：30 dBm

Receive antenna：8-element ULA

Element spacing=0.5wavelength

Bandwidth：120MHz

Time resolution：8.3ns

Antenna effective height

route no.1：1.8 m

route no.2：28.8 m

route no.3 and route no.4：21.6m

Propagation delay time：1.6 μs for route no.1.

6.4 μs for route no.2, route no.3 and route no.4

We name site-ij as the particular propagation condition i along the measurement distance in route -j i.e., site12 means the LOS condition along route no.2, site23 means the OLOS condition along route no.3, site34 means the NLOS condition along route no.4

The propagation environment at each site is described as the following table.

Table 1- descriptions of the propagation environment at each route.

| route no.	Propagation situation	Local environment
route no.1	LOS with open-area OLOS obstructed by trees and vehicles NLOS fully blocked by the Engineering Building	None
route no.2	LOS with local scatters and scatter radius 1m OLOS obstructed by trees, vehicles and pedestrians NLOS fully blocked by some buildings	Local scatters like vehicles, bikes vegetation and vendors
route no.3	LOS with open-area and remote scatters OLOS obstructed by some vehicles slightly NLOS fully blocked by gymnasium	Remote scatters composed of mountains, hills
route no.4	LOS with local scatters and scatter radius 2m OLOS obstructed by trees NLOS fully blocked by Science Building	Local scatters like vehicles, bikes vegetation, horticultural timbers that line along walkways and plants
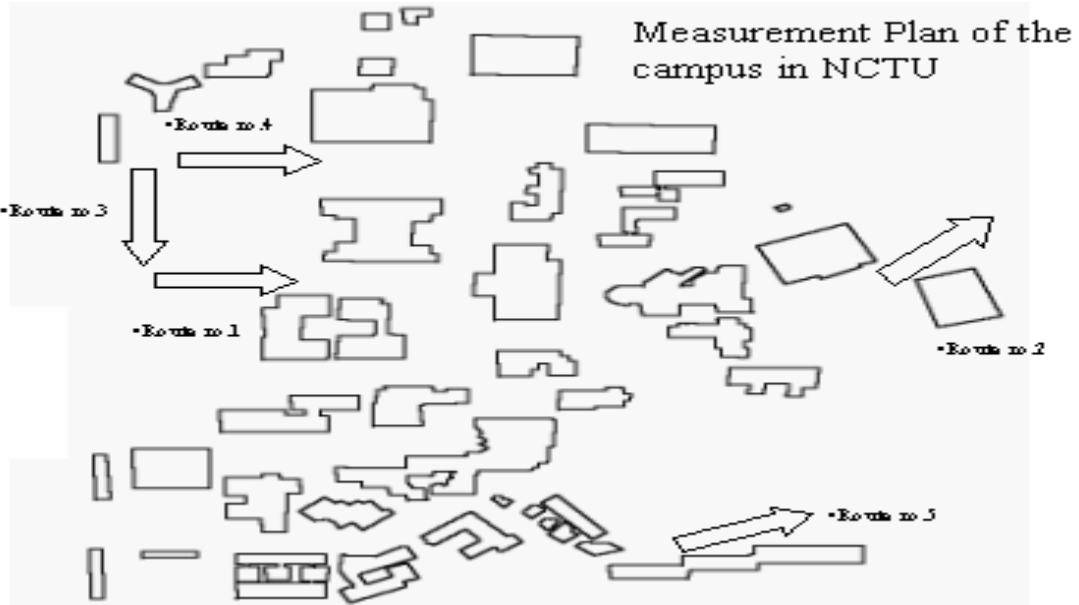
Fig. 3-3 Measurement sites in the NCTU campus

MIMO channels can be modelled either as double directional channels or as vector (matrix) channels. The former method is more related to the physical propagation effects, while the latter is more emphasized on the effect of the channel on the system. Another distinction is whether to treat the channel deterministically or stochastically. In the following, we outline the relations between those description methods.

The deterministic double directional channel is characterized by its double directional impulse response. It consists of L propagation paths between the transmitter and receiver sites. Each path is delayed in accordance to its excess-delay τ_i, weighted with the proper complex amplitude $a_i e^{j\Phi_i}$ and each direction of departure (AOD) $\Omega_{T,i}$ associated with the corresponding direction of arrival (AOA) $\Omega_{R,i}$. The channel impulse response matrix $\underline{h}$ is

$$\underline{h}(t,\tau,\Omega_T,\Omega_R) = \sum_l^L \underline{h}_l(t,\tau,\Omega_T,\Omega_R) = \sum_l^L \alpha_l e^{j\phi_l} \delta(\tau-\tau_l)\delta(\Omega-\Omega_{T,l})\delta(\varphi-\Omega_{R,l}) \quad (10)$$

In general, all multipath parameters：$\alpha_l, \tau_l, \Omega_{T,l}, \Omega_{R,l}$ and $e^{j\phi_l}$ will depend on the

24

absolute time t; also the set of multipath components (MPCs) contributing to the propagation will vary, N→N(t). The variations with time can occur both because of movements of scatters, and movement of the transmitter. The number of paths L can become very large if all possible paths are taken into account. In our experiments, the total number of resolvable multipath components was between 193 and 769. We simulate the deterministic channel applying the site-specific method to describe the direct wave, specular reflection waves, and single and multiple-over-rooftop diffracted waves. Once the site-specific method, i.e. deterministic method, is finished, the field strength distribution, power delay profile and power azimuth profile are shown in Fig. 3-4, we survey the multipaths in propagation, only one path is single rooftop diffracted wave accompanied with other 31 corner diffracted multipaths and acquire different realizations of the channel and proceed this procedure 15 times to obtain the complete channel matrix $H_{4\times4}$. Based on the theory of reciprocity of antenna, we obtain AOD by interchanging the position the transmitter and receiver. AOA Ω_T, AOD Ω_R in route no.1 case is approximately 0^0. Repeating the procedure above for 100 times gives an ensemble of channel realization and computes the capacity and plots a cumulative distribution function (CDF) for the MIMO channel capacity. Fig.3-4 gives the power delay profile and power azimuth profile of measurement for LOS of route no.1 and Fig 3-5 gives the time averaged Delay-Azimuth Spectrum of measurement of route no.1.
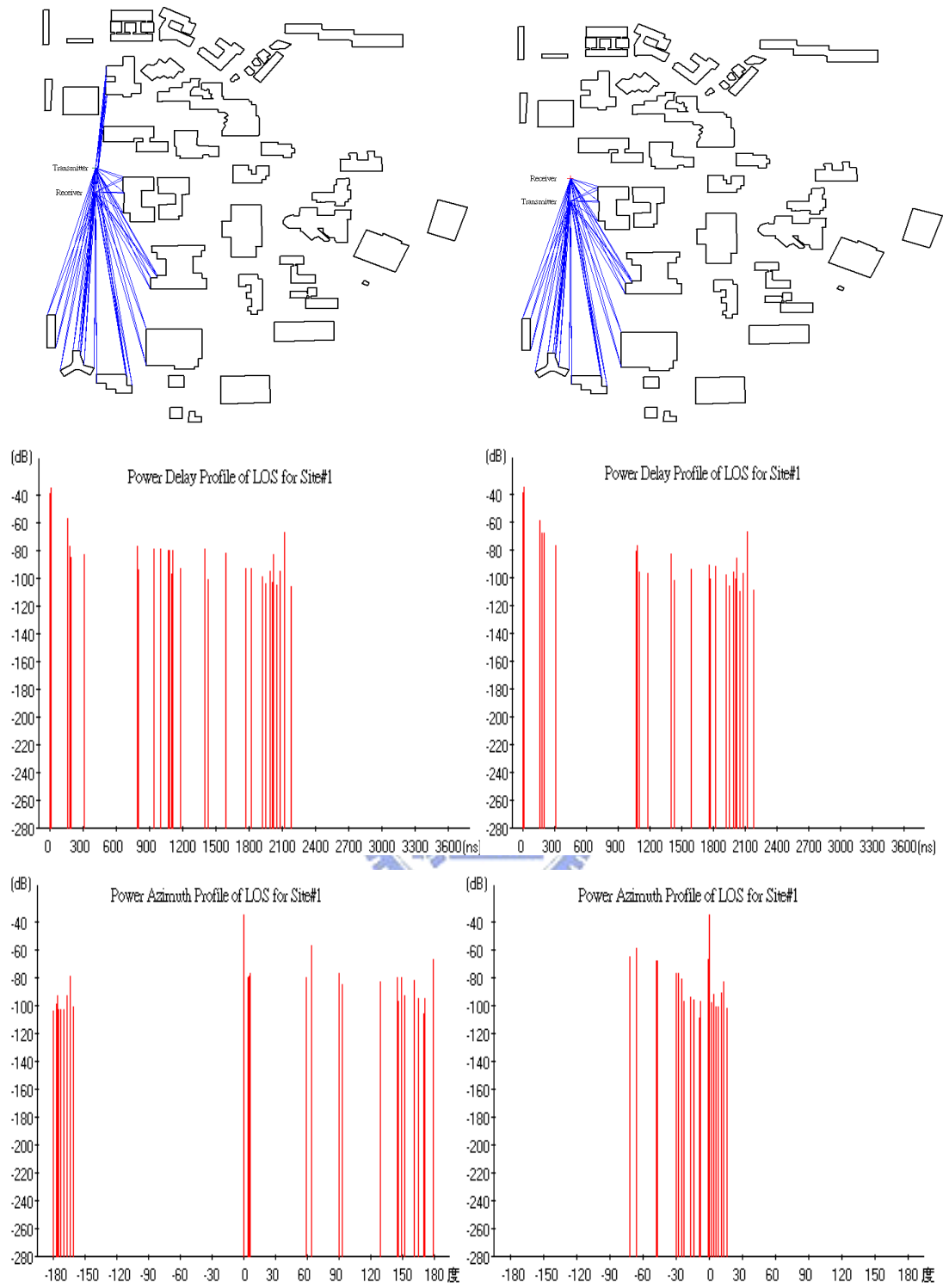
Fig 3-4. The field strength distribution of propagation, power delay profile and power azimuth profile for LOS of route no.1 in the left straight side, the ones which transmitter and receiver are interchanged shown in the right straight.
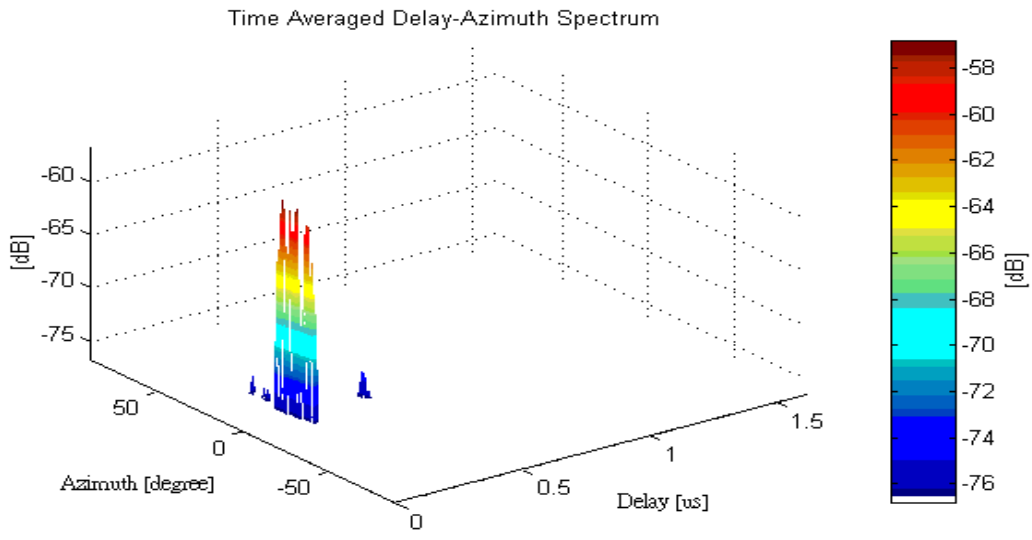
Fig 3-5 Time Averaged Delay-Azimuth Spectrum of measurement of route no.1
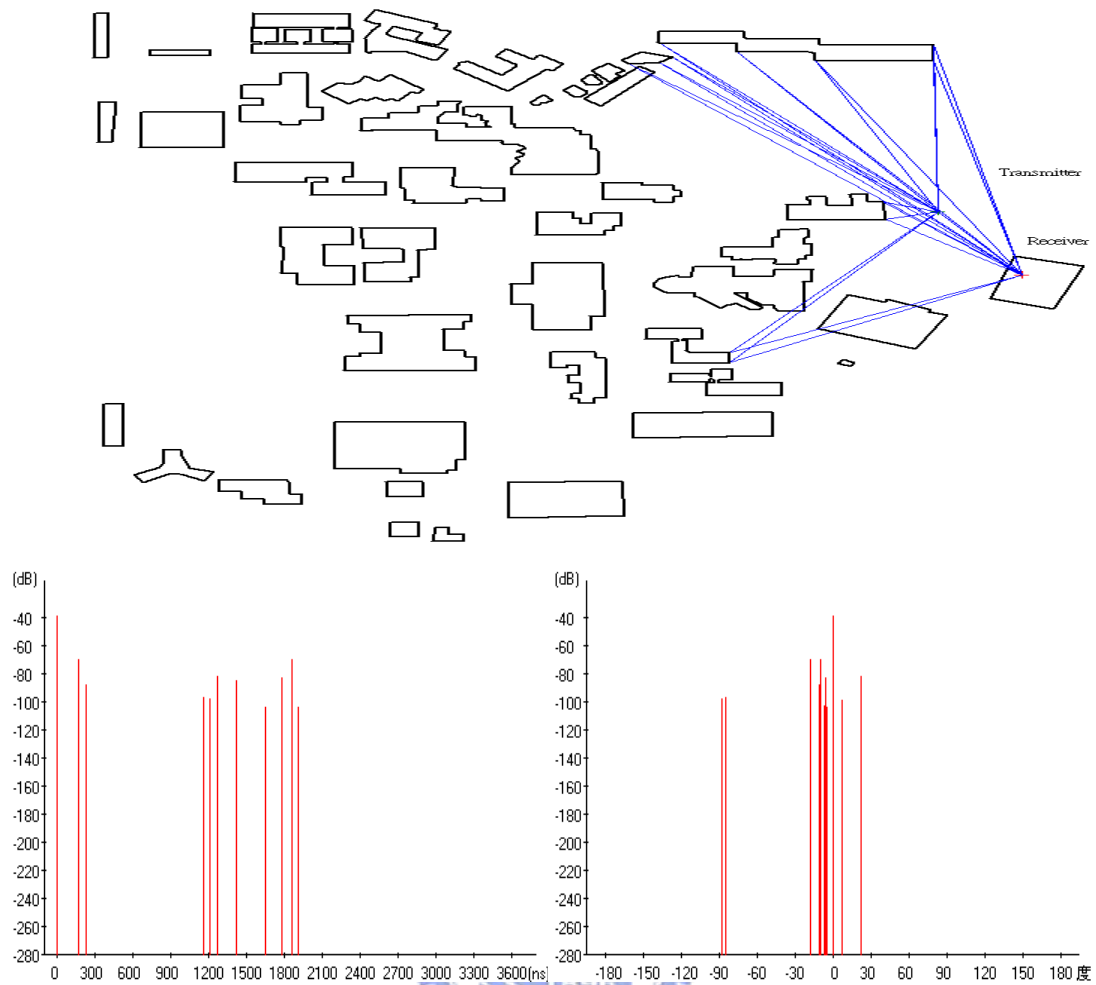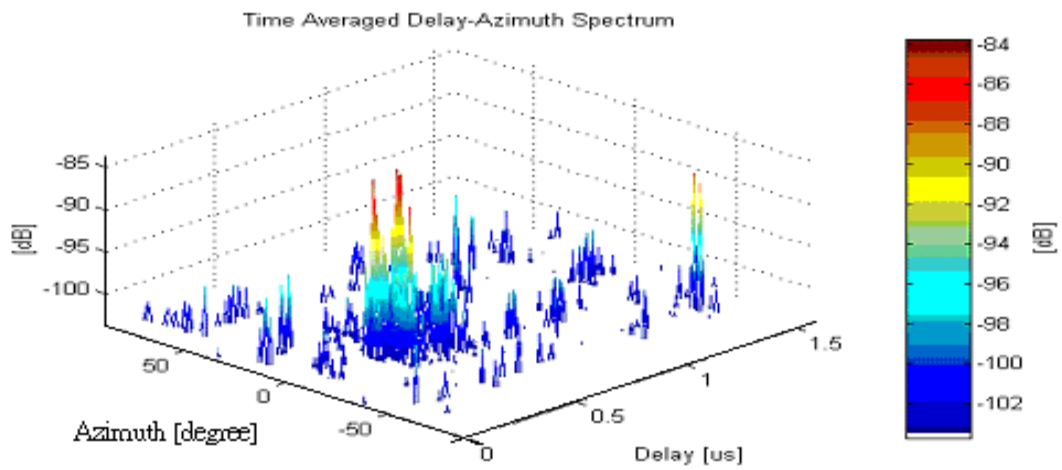
Fig 3-6 (a)

Fig 3-6 (b)
Fig 3-6 (a) Field strength distribution of route no.2 and the Power Delay Profile and Power Azimuth Profile of route no.2 (b) Time Averaged Delay-Azimuth Spectrum of measurement of route no.2

Fig 3-7 (a)

Fig 3-7 (b)

Fig 3-7 (a) Field strength distribution of route no.3 and the Power Delay Profile and Power Azimuth Profile of route no.3 (b) Time Averaged Delay-Azimuth Spectrum of measurement of route no.3

Fig 3-8 (a)

Fig 3-8 (b)

Fig 3-8 (a) Field strength distribution of route no.4 and the Power Delay Profile and Power Azimuth Profile of route no.4 (b) Time Averaged Delay-Azimuth Spectrum of measurement of route no.4
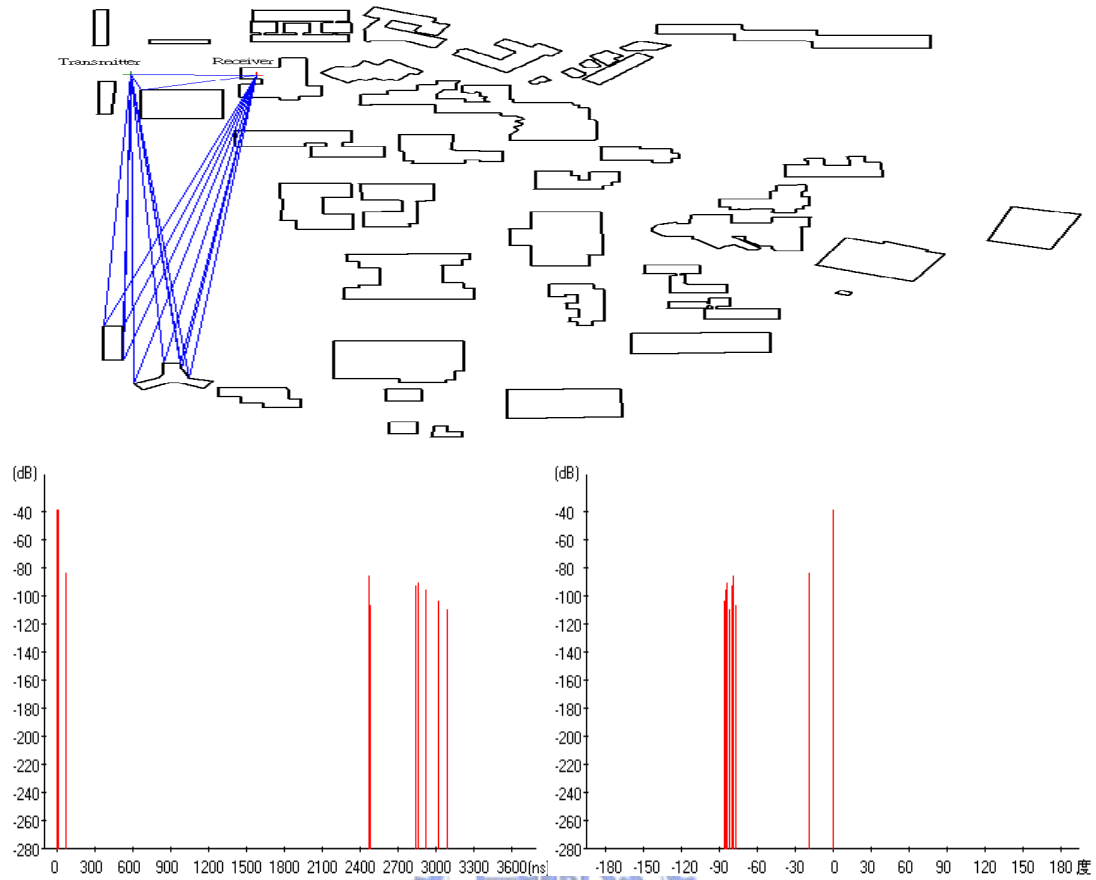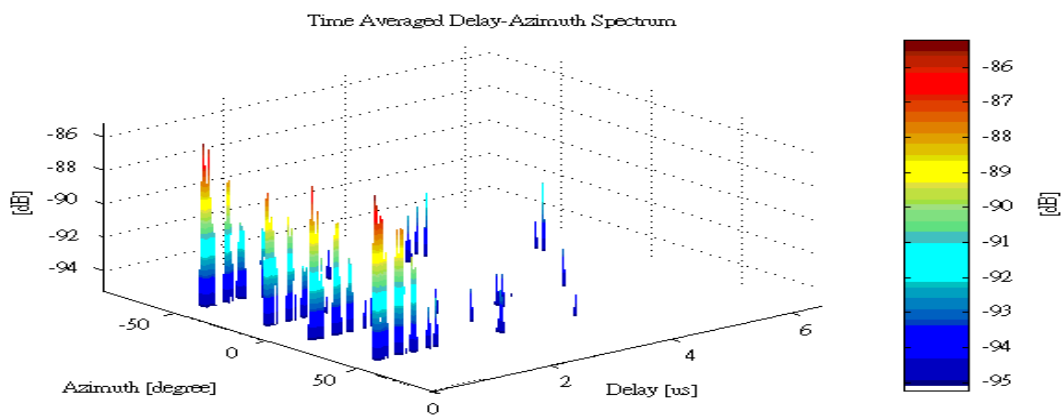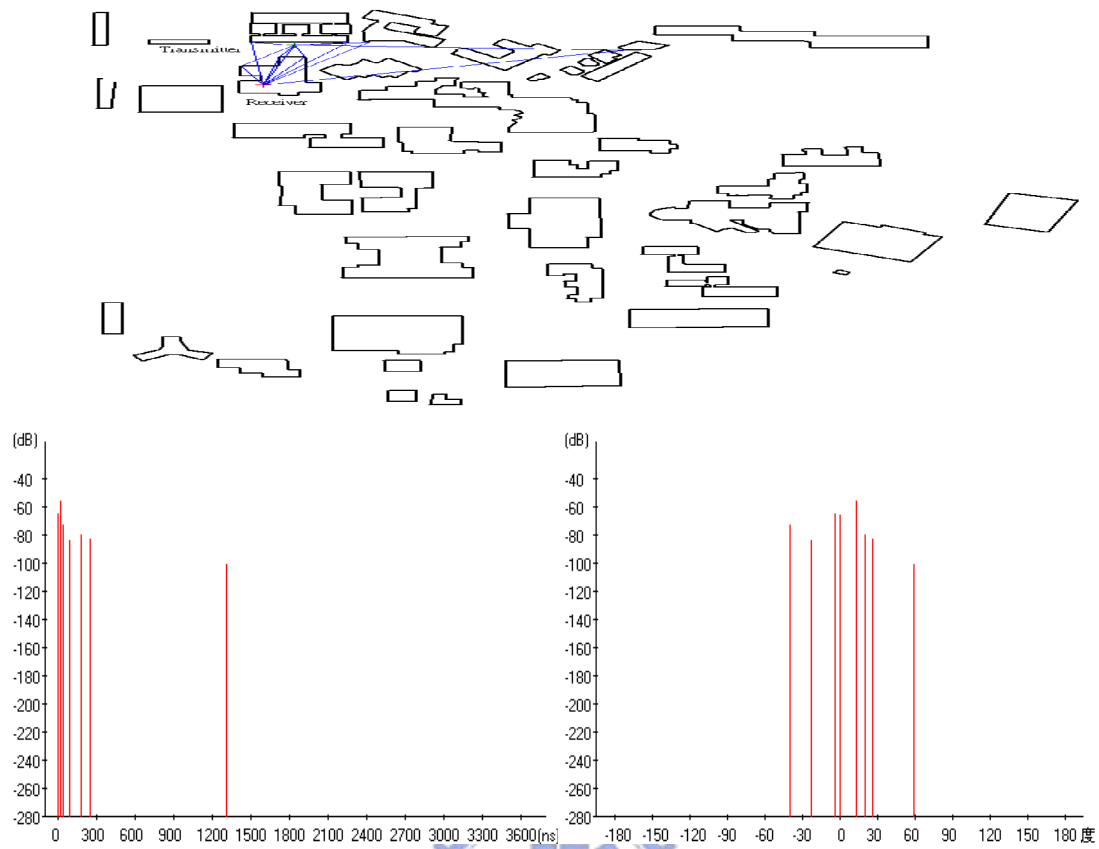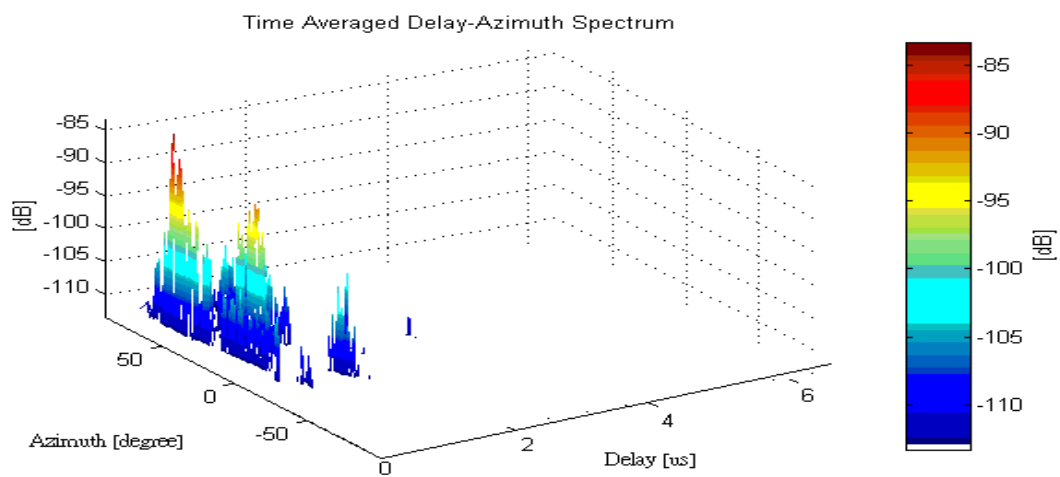
3.3 Measurement data extraction

By examining the measurement raw data, we extracted the angle-of-arrival (AOAs), angle-of-departure (AODs), delays and azimuths of the multipath components [10].

Using the commercial software "Matsys" to obtain

(1) Time-variant Impulse Response $h(t, \tau, s)$, where t represents observation time, τ represents delay time, s represent channel, we take this to evaluate whether the environment is "clean" i.e. observing the Power Delay Profile had a trend of decaying along the propagation distance as time is going. In Fig. 3-9, we observe that (a)~(c) power level increases as time goes by and (c) appear apparent decaying situation at some measurement, the same bandwidth. In Fig. 3-9 (c), there is a time difference between the strongest receive signal power and next strong one around 0.25~0.3us, i.e. the multipath propagate to arrival receive array more over 75~90m. From these Power Delay Profiles, we recognize (a)~(c) as OLOS, NLOS and LOS, respectively and take these snapshots for data processing.
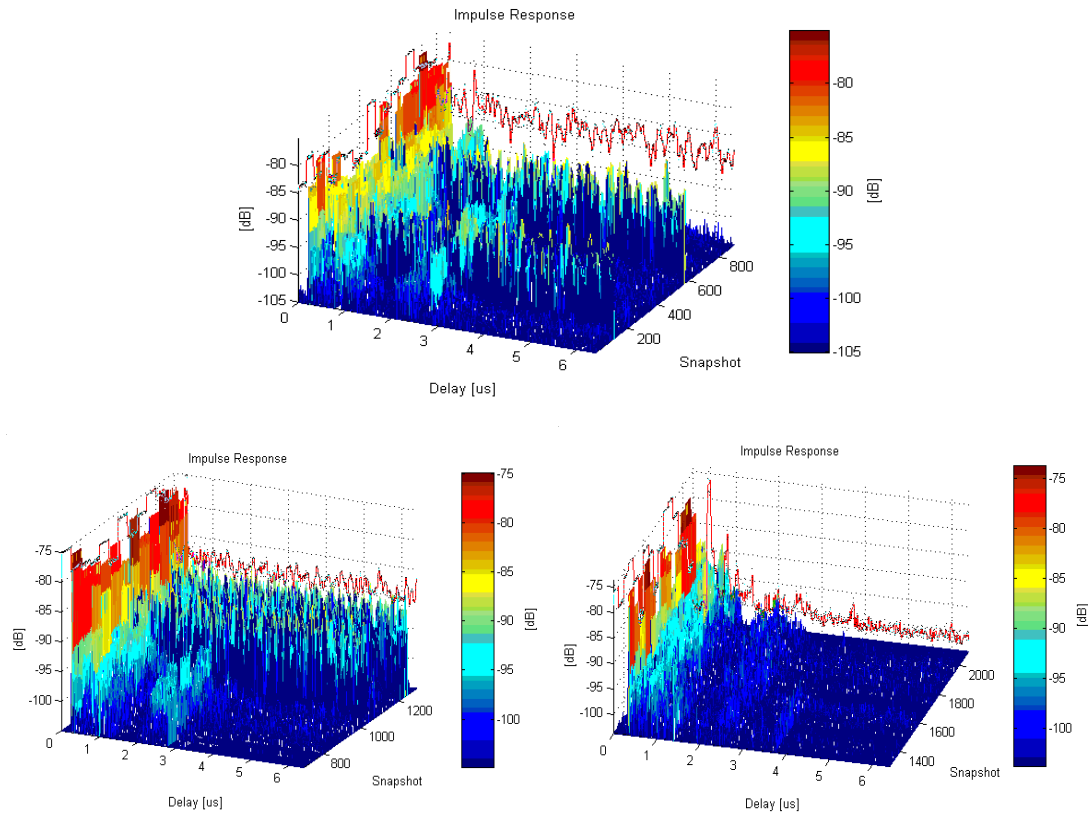
Fig. 3-9 The impulse response of (a) top (b) bottom left (c) bottom right figure
presents the measurement during different observation time

(2) Delay-Azimuth spectrum：extract multipath amplitudes from various azimuths and delays. We used Unitary ESPRIT (a parametric subspace estimation method incorporating forward-backward averaging) algorithm for detecting the information of direction to obtain time-variant delay-azimuth spread $h_{t,\tau,\Theta}(t,\tau,\Theta)$. There are two kind of sampling result：

Spatial sampling-for fixed τ (delay), extract multipath from various azimuths

Temporal sampling-for fixed ϕ (azimuth), extract multipath from various delay bins.

From these two processing, we are ready to compute the effective multipath number under some environment and root mean square delay spread and azimuth spread, which can be used to evaluate the dispersionness of propagation.

$$\text{Delay spread } (\sigma_\tau) = \sqrt{\frac{\sum_k P(\tau_k)\tau_k^2}{\sum_k P(\tau_k)} - \left(\frac{\sum_k P(\tau_k)\tau_k}{\sum_k P(\tau_k)}\right)^2}$$

$$\text{Azimuth spread } (\sigma_\phi) = \sqrt{\frac{\sum_k P(\phi_k)\phi_k^2}{\sum_k P(\phi_k)} - \left(\frac{\sum_k P(\phi_k)\phi_k}{\sum_k P(\phi_k)}\right)^2}$$

(3)Frequency response：H(t, f, s) to obtain the corresponding MIMO capacity.

According to the propagation delay time and measurement bandwidth, we obtain 193 (or 769) delay bins in the Power Delay Profile and 193 (or 769) multipaths in the time domain contribute to the capacity through the Fourier transform in the frequency domain illustrated in Fig. 3-10. From consecutive snapshots received by array, we take a bundle of snapshots, depends on the element spacing, total measurement distance and moving speed, for representing the signal bursted out from one transmit antenna. Take the data of route no.1 10λ element spacing at the transmit end for example, we need 312 snapshots to simulate the one transmit antenna, other three transmitter done in the same way. While the frequency responses from four transmitters are produced and averaged, we obtain a transfer channel matrix $H^{4x4x193}$ (or $H^{4x4x769}$) and normalize to $\sum_{i,j}\left|h_{ij}\right|^2 = 1$, the normalization of channel matrix is in order to remove the path loss, the superscript of 193 (or 769) represents the frequency bins resolved from bandwidth and then compute the capacity of each frequency bin based on (5). This concept is merely like the expression below

$$H_{4x4}^{(-60MHz)} = \begin{bmatrix} h_{11}^{(-60MHZ)} & h_{12}^{(-60MHZ)} & h_{13}^{(-60MHZ)} & h_{14}^{(-60MHZ)} \\ h_{21}^{(-60MHZ)} & h_{22}^{(-60MHZ)} & h_{23}^{(-60MHZ)} & h_{24}^{(-60MHZ)} \\ h_{31}^{(-60MHZ)} & h_{32}^{(-60MHZ)} & h_{33}^{(-60MHZ)} & h_{34}^{(-60MHZ)} \\ h_{41}^{(-60MHZ)} & h_{42}^{(-60MHZ)} & h_{43}^{(-60MHZ)} & h_{44}^{(-60MHZ)} \end{bmatrix} \rightarrow C_{4x4}^{(-60MHZ)}$$

$$\vdots$$

$$H_{4x4}^{(0MHz)} = \begin{bmatrix} h_{11}^{(0MHz)} & h_{12}^{(0MHz)} & h_{13}^{(0MHz)} & h_{14}^{(0MHz)} \\ h_{21}^{(0MHz)} & h_{22}^{(0MHz)} & h_{23}^{(0MHz)} & h_{24}^{(0MHz)} \\ h_{31}^{(0MHz)} & h_{32}^{(0MHz)} & h_{33}^{(0MHz)} & h_{34}^{(0MHz)} \\ h_{41}^{(0MHz)} & h_{42}^{(0MHz)} & h_{43}^{(0MHz)} & h_{44}^{(0MHz)} \end{bmatrix} \rightarrow C_{4x4}^{(0MHz)}$$

$$\vdots$$

$$H_{4x4}^{(60MHz)} = \begin{bmatrix} h_{11}^{(60MHZ)} & h_{12}^{(60MHZ)} & h_{13}^{(60MHZ)} & h_{14}^{(60MHZ)} \\ h_{21}^{(60MHZ)} & h_{22}^{(60MHZ)} & h_{23}^{(60MHZ)} & h_{24}^{(60MHZ)} \\ h_{31}^{(60MHZ)} & h_{32}^{(60MHZ)} & h_{33}^{(60MHZ)} & h_{34}^{(60MHZ)} \\ h_{41}^{(60MHZ)} & h_{42}^{(60MHZ)} & h_{43}^{(60MHZ)} & h_{44}^{(60MHZ)} \end{bmatrix} \rightarrow C_{4x4}^{(60MHz)}$$

We view the capacity of different frequency bins sas the contribution of multipath and

average it to obtain the corresponding array capacity for a sampled measurement.
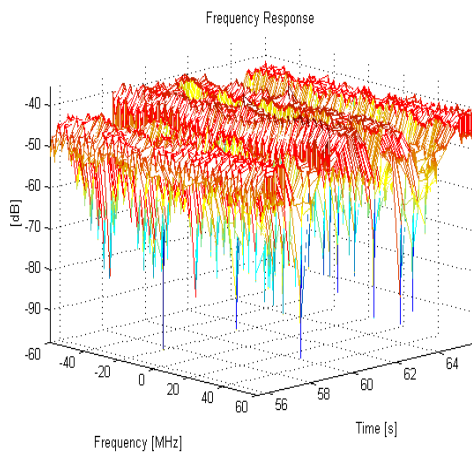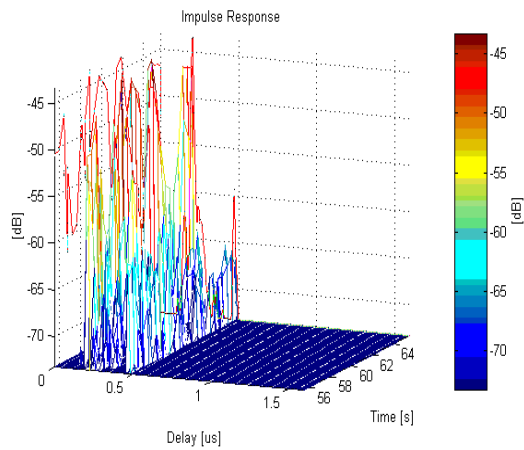

Fig 3-10 (a)   Fig 3-10 (b)

Fig. 3-10 The frequency response (a) and impulse response (b) of the channel

The procedures of Unitary ESPRIT to obtain AOA and AOD listed as below [11]：

1. Initialization：Form the matrix $\tilde{\underline{X}} \in C^{M \times N \times D}$ from the available measurement

   M represents an M-element sensor array composed of m pairs of pair-wise identical, but displaced sensors (doublets), i.e. M=4, N represent the number of selected snapshots, i.e. N=10, D represents the number of delay bins, i.e. D=193.

2. Signal Subspace Estimation：Determine the real matrix $T\{\tilde{\underline{X}}\} \in \mathfrak{R}^{M \times 2N \times D}$

$$T\{\tilde{\underline{X}}\}=\begin{bmatrix} \text{Re}\{\underline{G}_1 + \underline{\pi}\underline{G}_2\} & -\text{Im}\{\underline{G}_1 - \underline{\pi}\underline{G}_2\} \\ \sqrt{2}\,\text{Re}\{\underline{g}^T\} & -\sqrt{2}\,\text{Im}\{\underline{g}^T\} \\ \text{Im}\{\underline{G}_1 + \underline{\pi}\underline{G}_2\} & \text{Re}\{\underline{G}_1 - \underline{\pi}\underline{G}_2\} \end{bmatrix}$$

and compute the SVD of $T\{\tilde{\underline{X}}\}$ (square root approach) or the eigendecomposition of $T\{\tilde{\underline{X}}\}\,T\{\tilde{\underline{X}}\}^H$ (covariance approach). The d dominant left singular vectors or eigenvectors will be called $\underline{E}_s \in \mathfrak{R}^{M \times d \times D}$. Estimate the number of sources d, if d is not a priori.

   We consider an efficient computation of a particular transformation T ($\cdot$). It transforms an arbitrary complex matrix $X \in C^{p \times q}$ into a real p x 2q matrix, denoted by T (X). The block matrices G_1 and G_2 should have the same size, we set them as G_1 and $G_2 \in C^{2 \times 5}$, π_2 represent the 2 x 2 exchange matrix with ones on its antidiagonal and zeros elsewhere, i.e. $\pi_2 = \begin{bmatrix} 0 & 1 \\ 1 & 0 \end{bmatrix}$, $g^T = 0$ since M is even. Then an efficient computation of $T\{\tilde{\underline{X}}\} \in \mathfrak{R}^{M \times 2N \times D}$ from the matrix $\tilde{\underline{X}}$ only requires p x 2q real additions. Notice that $d \leq N$.

3. (Total) Least Squares：Solve the overdetermined system of equations

$$\underline{\kappa}_1 \underline{E}_s \gamma \approx \underline{\kappa}_2 \underline{E}_s$$

by means of least square techniques.

35

$$\underline{\kappa}_1 = \underline{Q}_m^H (\underline{J}_1 + \pi_m \underline{J}_1 \pi_M) \underline{Q}_M$$

$$\underline{\kappa}_2 = \underline{Q}_m^H j(\underline{J}_1 - \pi_m \underline{J}_1 \pi_M) \underline{Q}_M$$

where $Q_{2n} = \dfrac{1}{\sqrt{2}} \begin{bmatrix} I_n & jI_n \\ \pi_n & -j\pi_n \end{bmatrix}$ and $Q_{2n+1} = \dfrac{1}{\sqrt{2}} \begin{bmatrix} I_n & 0 & jI_n \\ 0^T & \sqrt{2} & 0^T \\ \pi_n & 0 & -j\pi_n \end{bmatrix}$

we choose the size of subarray as 3, i.e. m=3, Q_3 is the unitary matrix, J_1 is the

selection matrix given by $Q_3 = \dfrac{1}{\sqrt{2}} \begin{bmatrix} 1 & 0 & j \\ 0 & \sqrt{2} & 0 \\ 1 & 0 & -j \end{bmatrix}$, $J_1 = \begin{bmatrix} 1 & 0 & 0 & 0 \\ 0 & 1 & 0 & 0 \\ 0 & 0 & 1 & 0 \end{bmatrix}$ and,

$Q_4 = \dfrac{1}{\sqrt{2}} \begin{bmatrix} 1 & 0 & j & 0 \\ 0 & 1 & 0 & j \\ 0 & 1 & 0 & -j \\ 1 & 0 & -j & 0 \end{bmatrix}$, then we will obtain

$\kappa_1 = \begin{bmatrix} 1 & 1 & 0 & 0 \\ 0 & \sqrt{2} & 0 & 0 \\ 0 & 0 & 1 & 1 \end{bmatrix}$ and $\kappa_2 = \begin{bmatrix} 0 & 0 & -1 & 1 \\ 0 & 0 & 0 & -\sqrt{2} \\ 1 & -1 & 0 & 0 \end{bmatrix}$

4. Eigenvalue decomposition： Compute the eigenvalue decomposition of resulting

solution

$$\gamma = \underline{T}\underline{\Omega}\underline{T}^{-1} \in \Re^{d \times d}$$

where $\underline{\Omega} = \text{diag}\{w_k\}_{k=1}^{d}$ eigenvalue matrix and $w_k = \exp(-j\dfrac{w_0 d_t}{c}\sin(\theta_k))$

Chapter 4

Propagation and Antenna Arrangement Effects on MIMO Capacity

4.1 Propagation effect

Propagation at different conditions such as LOS, OLOS and NLOS may influence MIMO capacity. Here, we analyze the measured result along each route to see how the capacity changes as the conditions, propagation distance or local scatterer distribution varies, which is shown in section 4.1.1. Comparison between the measured result and the computed results from the ray-tracing based hybrid model will help to investigate the coupling effect between the element spacing and local scattering on the MIMO capacity. This is illustrated in section 4.1.2.
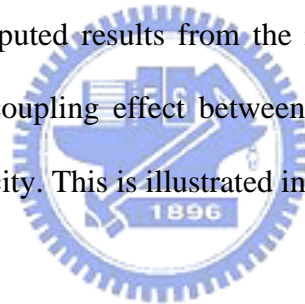
4.1.1 Measured result analysis

Figure 4-1 illustrates three CDFs of the measured MIMO capacity for LOS, OLOS and NLOS conditions along route no.1. There are three CDF curves to show the results of LOS, OLOS and NLOS conditions. The averaged capacity is 13.1102 bps/Hz for LOS condition, 14.9382 bps/Hz for OLOS condition and 15.65 bps/Hz for NLOS condition. It is found that the capacity in the LOS condition is smaller than that of the OLOS or NLOS condition. It is because that the rms AOA angular spread of the LOS condition is smaller than that of latter two conditions. The larger multipath angular dispersion will lead to less spatial correlation between receiving signals, i.e., larger capacity. This result is shown in Figure 4-2 where larger rms angle spread leads to larger capacity. Figures 4-3(a), (b) and (c) demonstrates the histograms of MIMO

capacity of LOS, OLOS and NLOS conditions, respectively. Similar results are found in the figure 4-4 for route no.2, figure 4-5 for route no.3 and figure 4-6 for route no.4.
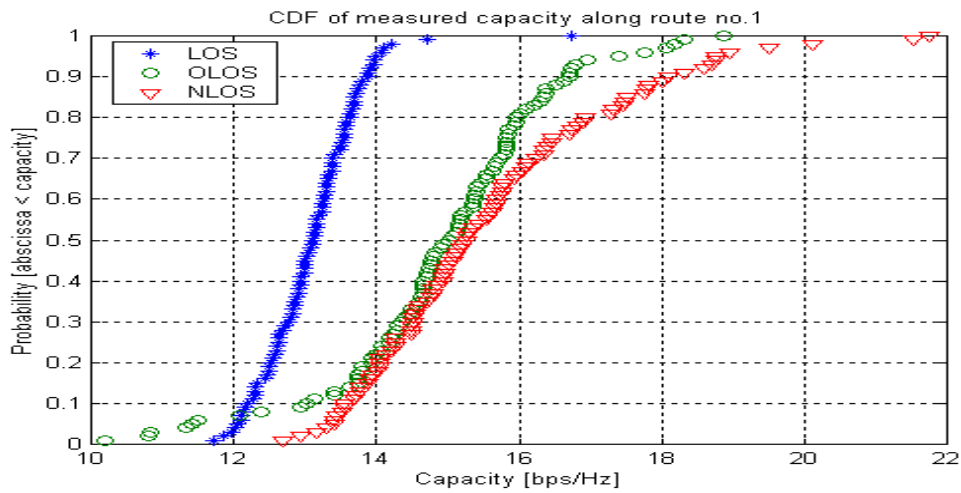

Fig 4-1 The CDF of the measured MIMO capacity for LOS (*), OLOS (o) and NLOS (∇) conditions along route no.1. The averaged capacity is 13.1102 bps/Hz for LOS condition, 14.9382 bps/Hz for OLOS condition and 15.65 bps/Hz for NLOS condition.
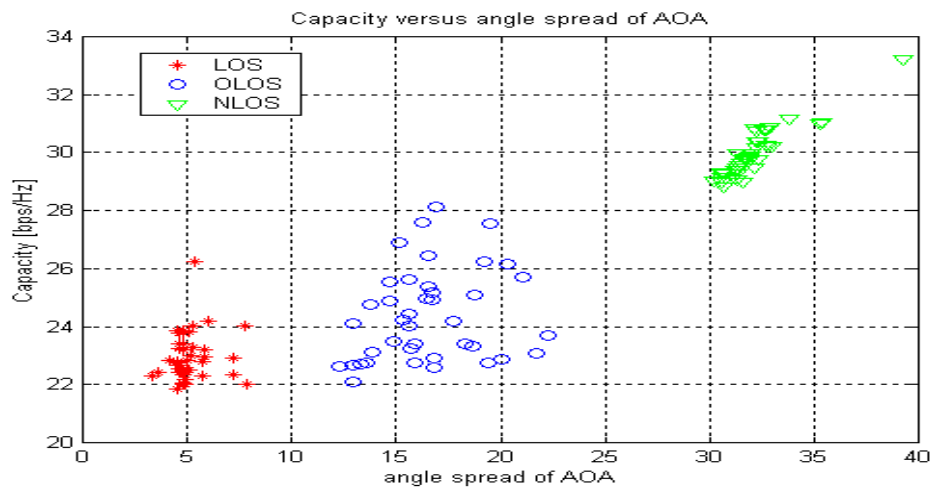

Fig 4-2 capacity versus rms angular spread of AOA for LOS (*), OLOS (o) and NLOS (∇) conditions
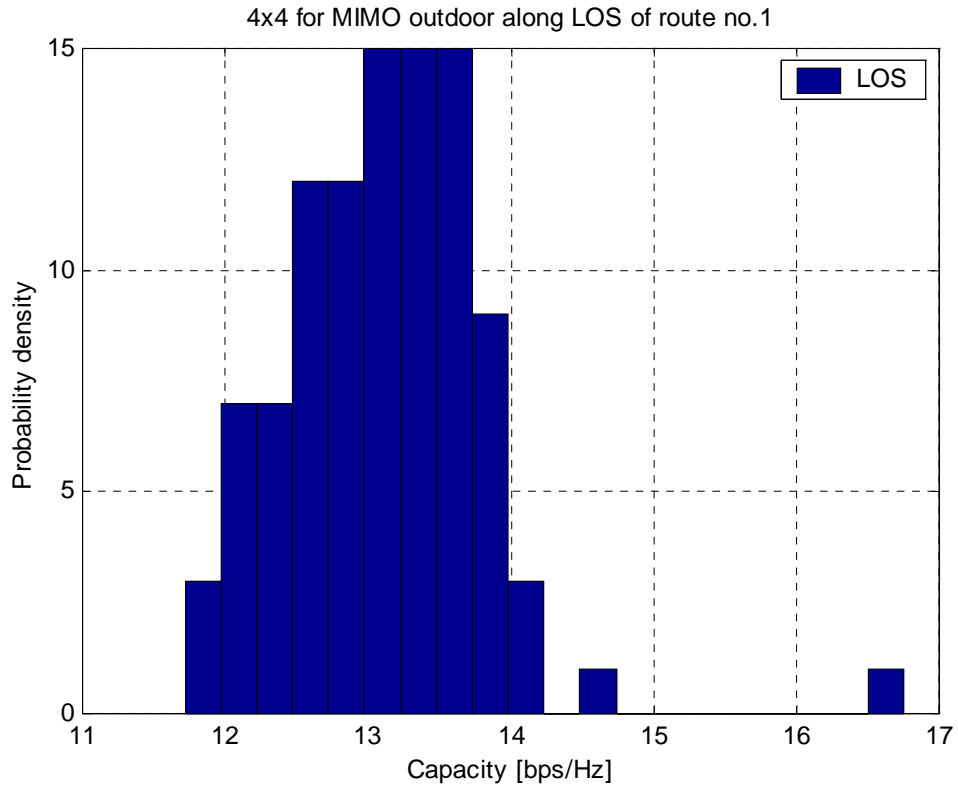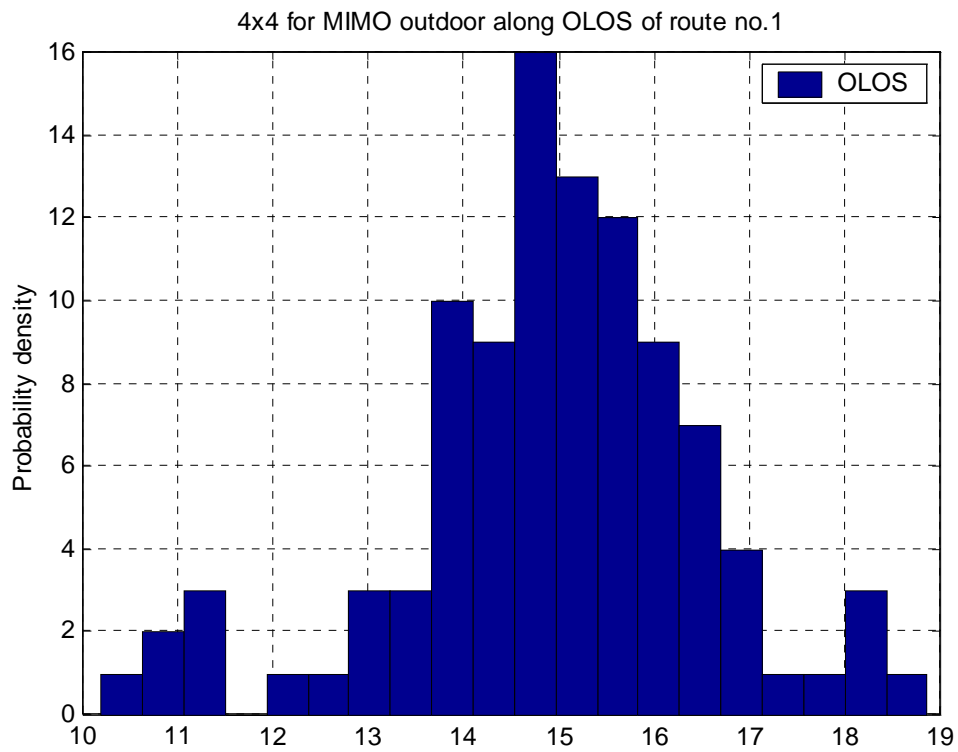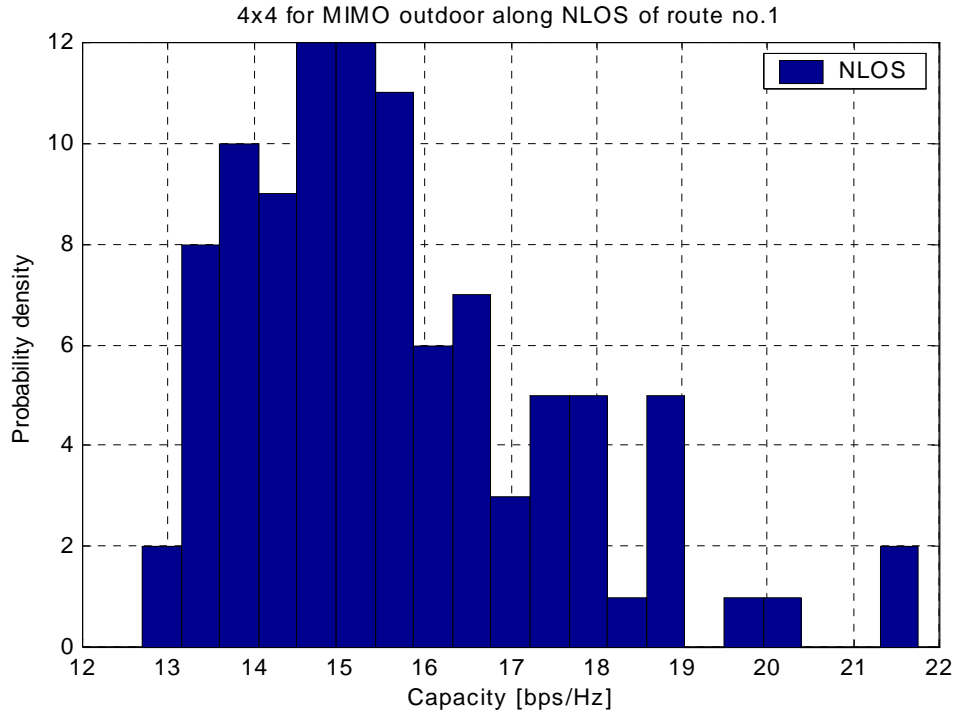
Fig 4-3 (a)

Fig 4-3 (b)

Fig 4-3 (c)

Figure 4-3 The histogram of MIMO capacity for (a) LOS, (b) OLOS and (c) NLOS conditions.

Fig 4-4 The CDF of the measured MIMO capacity for LOS (*), OLOS (o) and NLOS (∇) conditions along route no.2. The averaged capacity is 23.258 bps/Hz for LOS condition, 24.623 bps/Hz for OLOS condition and 24.8787 bps/Hz for NLOS condition.

Fig 4-5 The CDF of the measured MIMO capacity for LOS (*), OLOS (o) and NLOS (∇) conditions along route no.3. The averaged capacity is 21.7373 bps/Hz for LOS condition, 23.8253 bps/Hz for OLOS condition and 25.732 bps/Hz for NLOS condition.
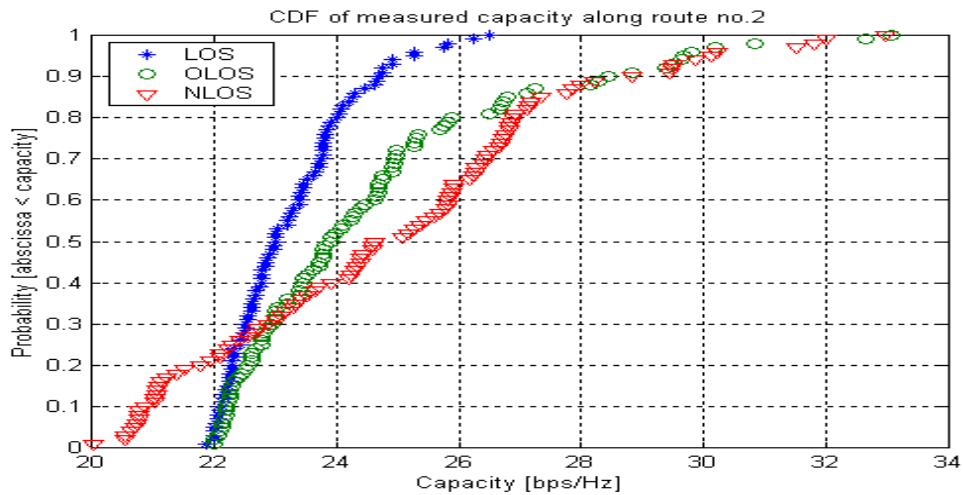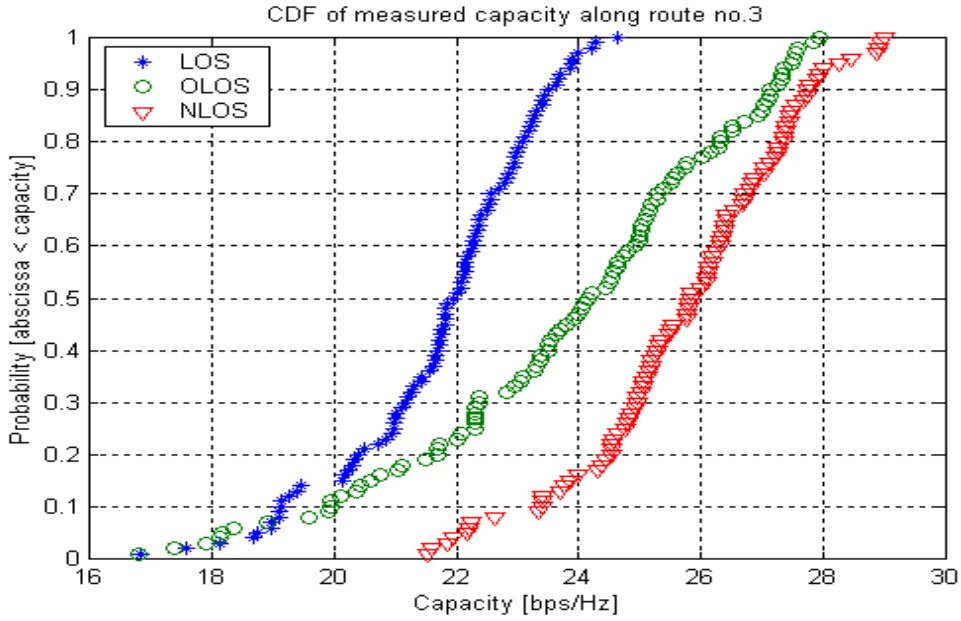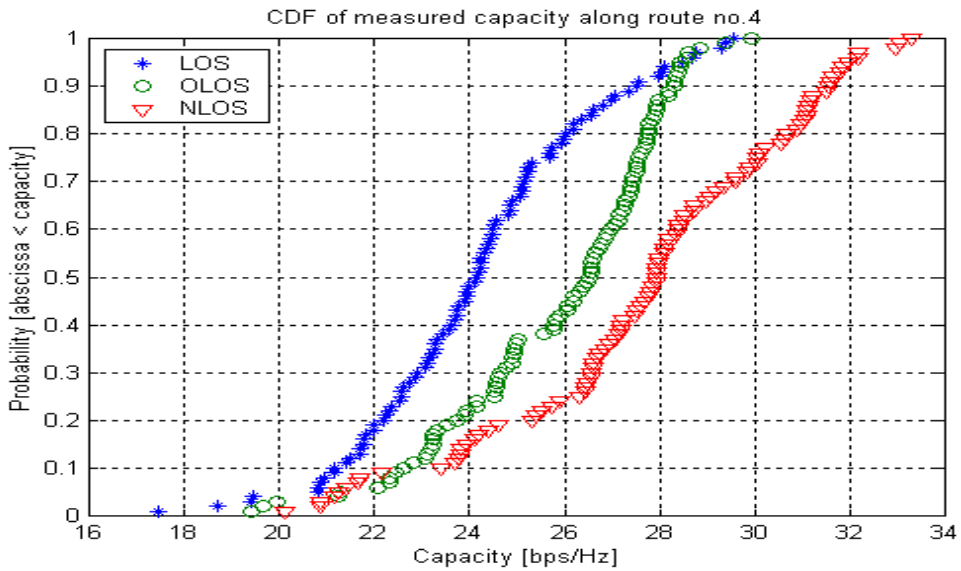

Fig 4-6 The CDF of the measured MIMO capacity for LOS (*), OLOS (o) and NLOS (∇) conditions along route no.4. The averaged capacity is 24.1806 bps/Hz for LOS condition, 25.8532 bps/Hz for OLOS condition and 27.6917 bps/Hz for NLOS condition.

4.1.2 Comparison among different routes

Fig 4-7 (a)~(c) illustrates the CDF of capacity of different routes for LOS, OLOS and NLOS respectively. From these three figures, we can obtain that the capacity performance of route no.1 is always smaller than that of others despite the LOS, OLOS and NLOS conditions. The performance of MIMO capacity along route no.2, route no.3 and route no.4 has some degree of resemblance. Since the distinctions of the measurement in the route no.1 with that of other three are the propagation distance and local scatterers, so we sample the capacity from measurement along the propagation distance for each route shown as Fig 4-8 and apply hybrid model shown as Fig 4-9 to investigate the effect of propagation distance on the capacity performance. In the same way, we compare Fig 4-10 with the figure applying hybrid model shown as Fig 4-11 for each route to investigate the effect of local scatterers on the capacity performance.
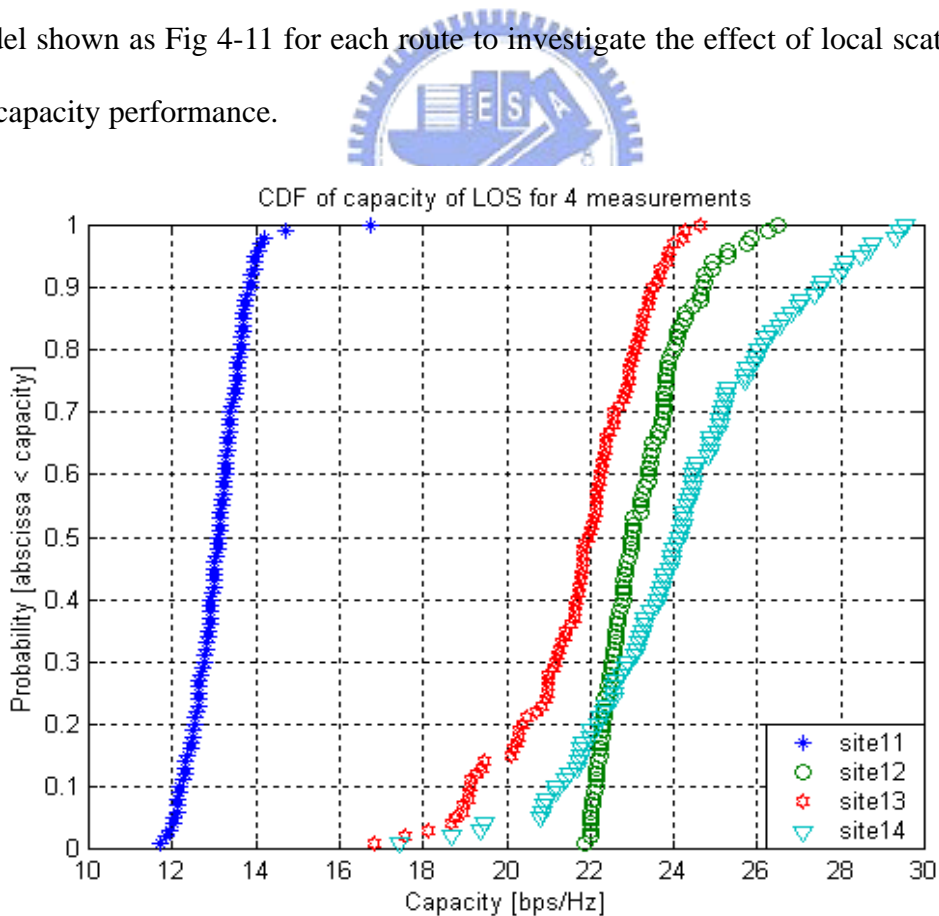
Fig 4-7 (a)
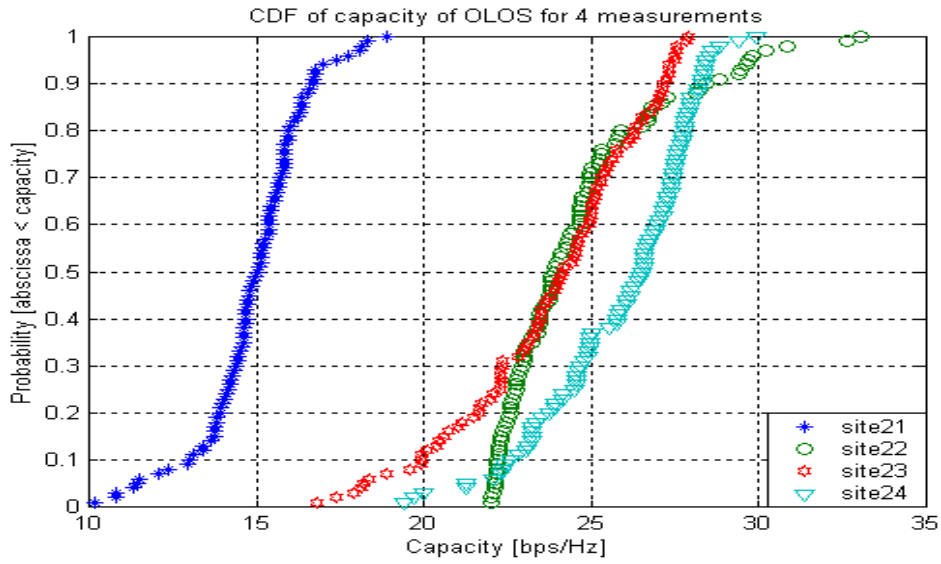
Fig 4-7 (b)
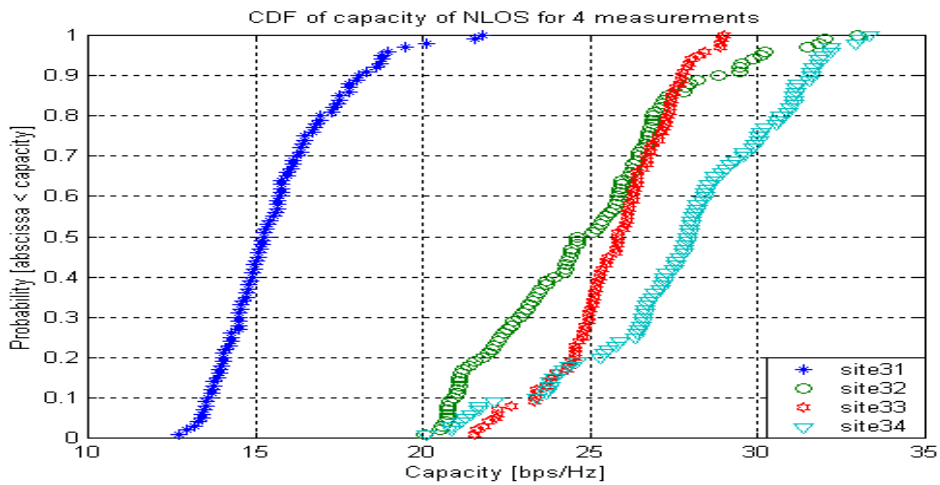
Fig 4-7 (c)

Fig. 4-7 (a) The CDF of capacity of LOS in each route, (b) the CDF of capacity of OLOS in each site and (c) the CDF of capacity of NLOS in each site. There are four CDF curves to show the results of LOS condition of route no.1, route no.2, route no.3 and route no.4 in Fig 4-7 (a), four CDF curves to show the results of OLOS condition of route no.1, route no.2, route no.3 and route no.4 in Fig 4-7 (b) and four CDF curves to show the results of NLOS condition of route no.1, route no.2, route no.3 and route no.4 in Fig 4-7 (c).

Fig 4-8 obviously presents that the capacity performance of shorter propagation distance 50m is indeed inferior to the one of other longer propagation distance. It despitse that propagation distance effect at each route does not exhibit regular trend and larger capacity deviation. Another information given by Fig 4-8 is that the standard deviation of capacity of propagation distance 50m is the smallest among the measurement results. This phenomenon tells us that transmitted signals through longer propagation distance may experience more complex channel so that causing more multipaths in the channel. In this way, the transmitted signals received by the opposite array will be less correlated each other, resulting in larger capacity fluctuation. Fig 4-9 shows that the computed results of CDF of the measurement along propagation distance. All are resembled except one in asterisk line sampled from route no.1 along propagation distance 50m.

Fig 4-10 shows the capacity variation of the LOS condition of measurements in all routes. It also provides us with the information of standard deviation of capacity sampled from all measurements, although the standard deviation of capacity in route no.1 is almost equal to the one in route no.3, the averaged capacity of measurements along route no.1 is much smaller than that of measurements along route no.3. This phenomenon can be explained as that the LOS condition around the route no.1 belongs to open-area and short distance, while the LOS condition around route no.3 characterized by distant scatters backed up with hills so that the transmitted signal propagated within quite small rms angular spread of AOA to the receive array. Otherwise, in the cases of route no.2 and route no.4, the capacity fluctuation differs from that of route no.1 and route no.3 significantly. Since the local scatterers like vehicles and pedestrians surrounded the transmitter in the LOS of route no.2 and route no.4 so that the transmitted signals within an extremely large rms angular spread of

AOA propagated to the receive array, resulting in transmitted signals less correlated each other. That is why the standard deviations of capacity of route no.2 and route no.4 vary dramatically. Fig 4-11 shows the computed results of CDF of LOS with local scatters in all measurements plus the case of LOS in route no.1 without local scatterer. From figure 4-8 to 4-11, we conclude that the propagation distance and local scatterers around transmit end array will affect the capacity performance.
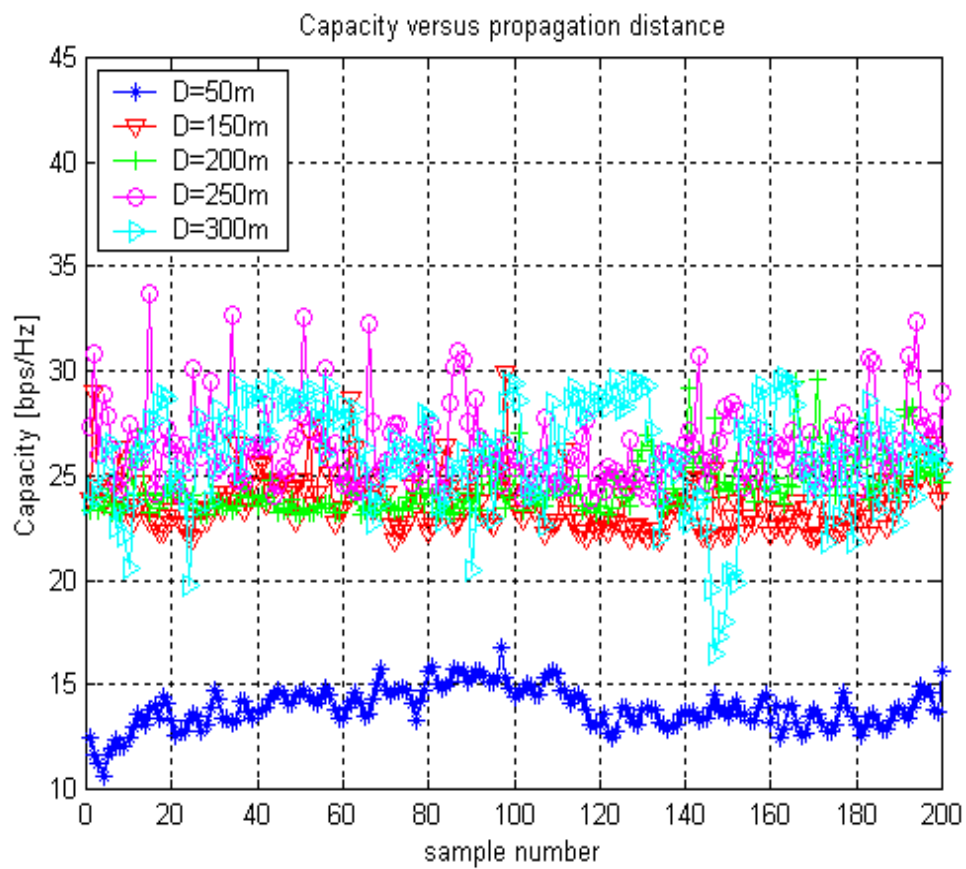

Fig 4-8 The capacity variation of different propagation distance D from measurement with standard deviation of the capacity $\sigma_{C,D=50m} = 0.9568$ bps/Hz, $\sigma_{C,D=150m} = 1.3368$ bps/Hz, $\sigma_{C,D=200m} = 1.2761$ bps/Hz, $\sigma_{C,D=250m} = 1.8584$ bps/Hz and $\sigma_{C,D=300m} = 2.5649$ bps/Hz.
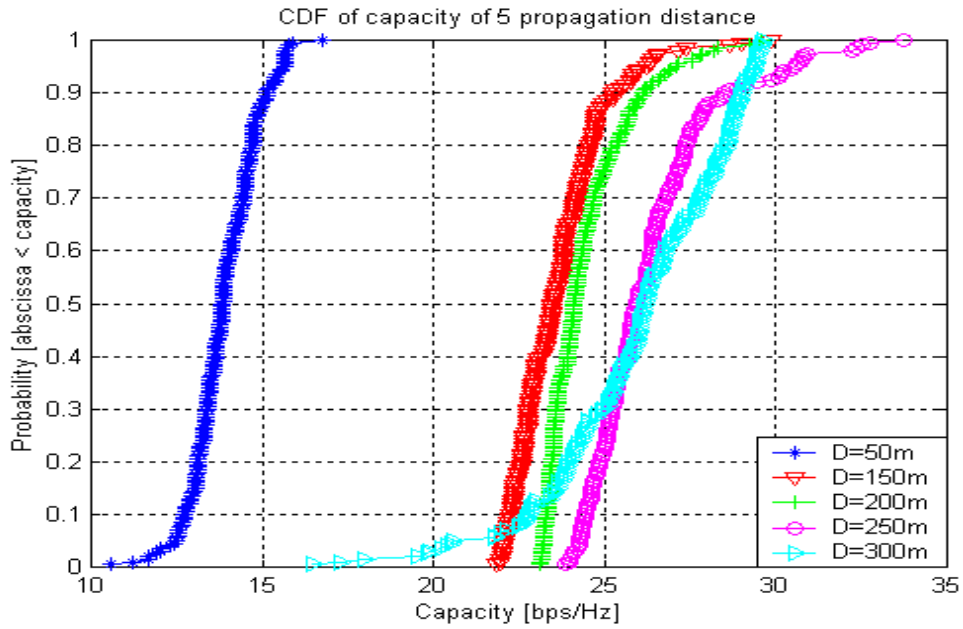
Fig 4-9 The CDF of capacity for different propagation distance applying hybrid model
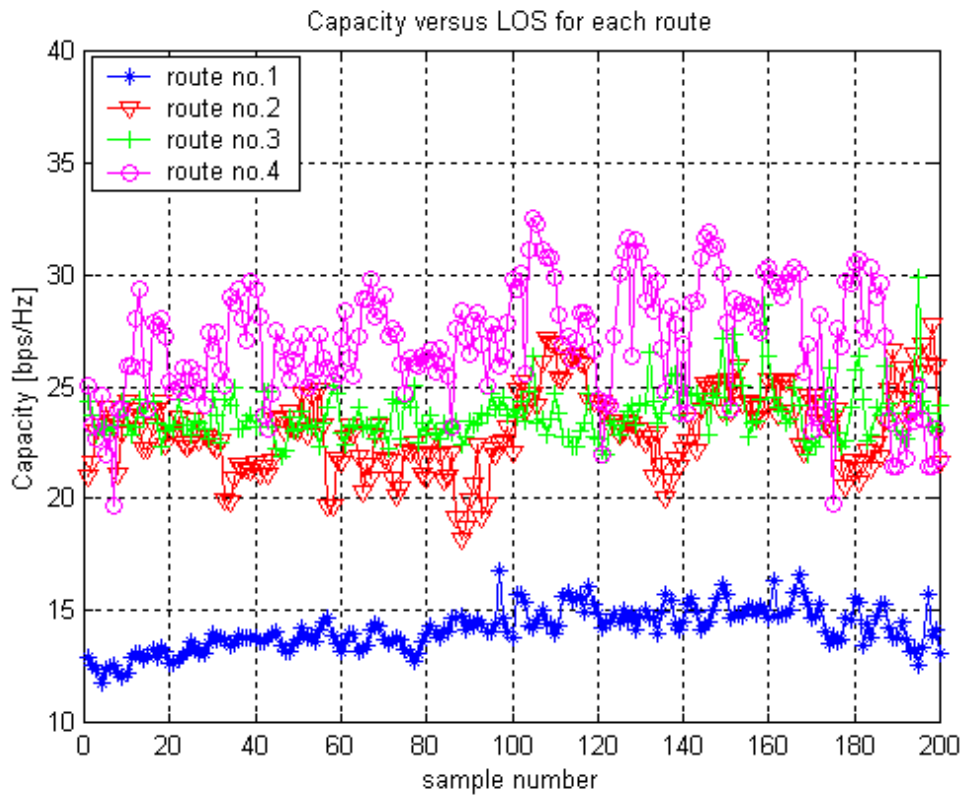
Fig 4-10 The capacity variation of LOS along different routes with standard deviation of capacity $\sigma_{C,route\ no.1} = 0.718$ bps/Hz, $\sigma_{C,route\ no.2} = 1.3745$ bps/Hz, $\sigma_{C,route\ no.3} = 0.7187$ bps/Hz and $\sigma_{C,route\ no.4} = 1.8458$ bps/Hz.
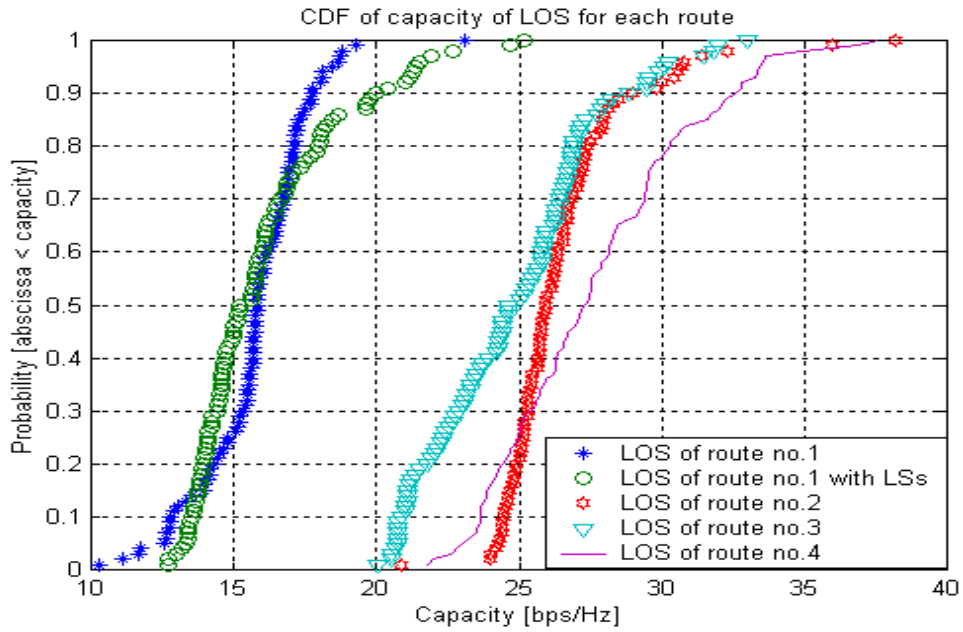
Fig 4-11 The computed CDF of the MIMO capacity for routes no.1-4 by using the hybrid model.

Fig 4-12 shows the averaged capacity of each route. It is found that in every route the capacity of LOS condition is always smaller than that of the OLOS or NLOS condition. It is because that the existence of direct path will reduce the rank of the channel matrix, which becomes a dominant factor in reducing the MIMO capacity.
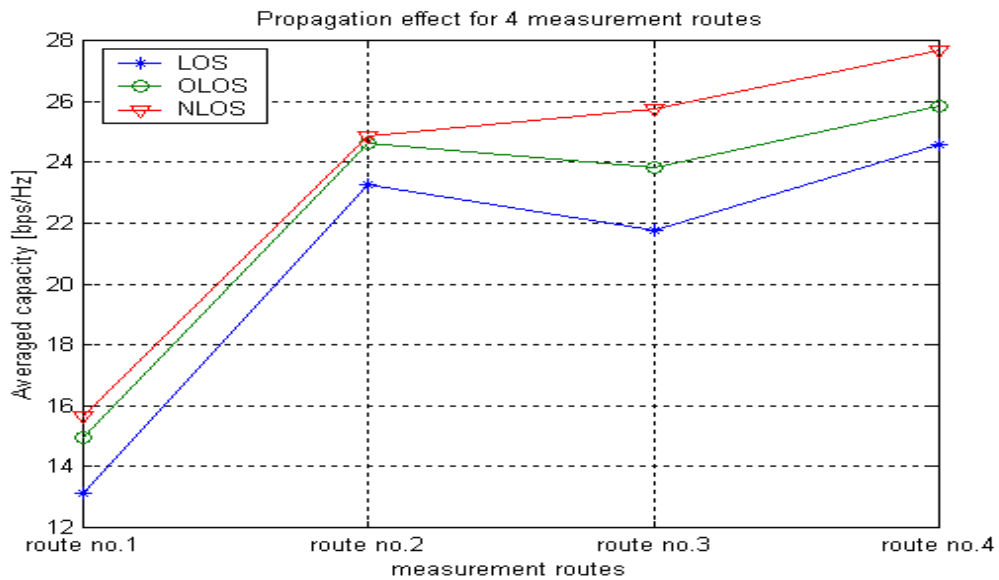
Fig 4-12 The averaged MIMO capacity for each route.

4.2 Element spacing effect

In this section, we investigate the impact of MIMO element spacing on capacity through the measured data. Comparison between the measurement result and the computed results using the ray-tracing based hybrid model will help to investigate the coupling effects between the element spacing and local scatterers on the MIMO capacity. Section 4.2.1 will introduce the measurement of MIMO element spacing for LOS, OLOS and NLOS conditions. Section 4.2.2 provides the computation results using the hybrid model. Section 4.2.3 compares the measurement and computed MIMO capacity.

4.2.1 Measurement Result Analysis

Fig 4-14 gives the capacity variation under LOS with MIMO element spacing for route no.1 and Fig 4-15 corresponding CDF of different element spacing. Figure 4-14 indicates that the capacity increases as the element spacing increases. Since the element spacing increases, the array aperture is approximately M x d_t, beamwidth is inversely proportional to aperture and resolution is inversely proportional to beamwidth, hence the larger array (d_t larger) resolves multipaths more, the propagation of MIMO channel filled with multipaths lead to the capacity to increases. Figures 4-16 (a), (b) and (c) demonstrates the histograms of MIMO capacity with element spacing $\Delta = 10\lambda \sim 30\lambda$ along route no.1, respectively. Similar results are found in the figure 4-17 (a) for route no.2, figure 4-17 (b) for route no.3 and figure 4-17 (c) for route no.4.
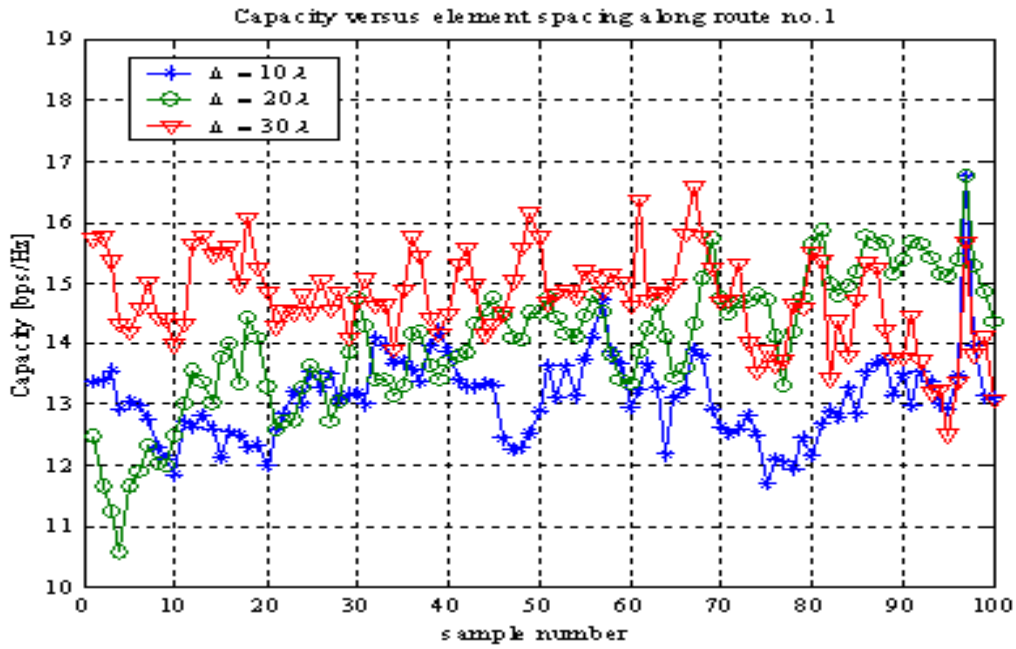
Fig 4-14 The capacity variation under LOS with MIMO element spacing for route no.1 with standard deviation of capacity $\sigma_{C,\Delta=10\lambda} = 0.7009$ bps/Hz, $\sigma_{C,\Delta=20\lambda} = 1.1148$ bps/Hz and $\sigma_{C,\Delta=30\lambda} = 0.7592$ bps/Hz

Fig 4-15 The CDF of different element spacing for LOS along route no.1. The averaged capacity is 13.1102 bps/Hz for $\Delta = 10\lambda$ condition, 14.0516 bps/Hz for $\Delta = 20\lambda$ condition and 14.7373 bps/Hz for $\Delta = 30\lambda$ condition.
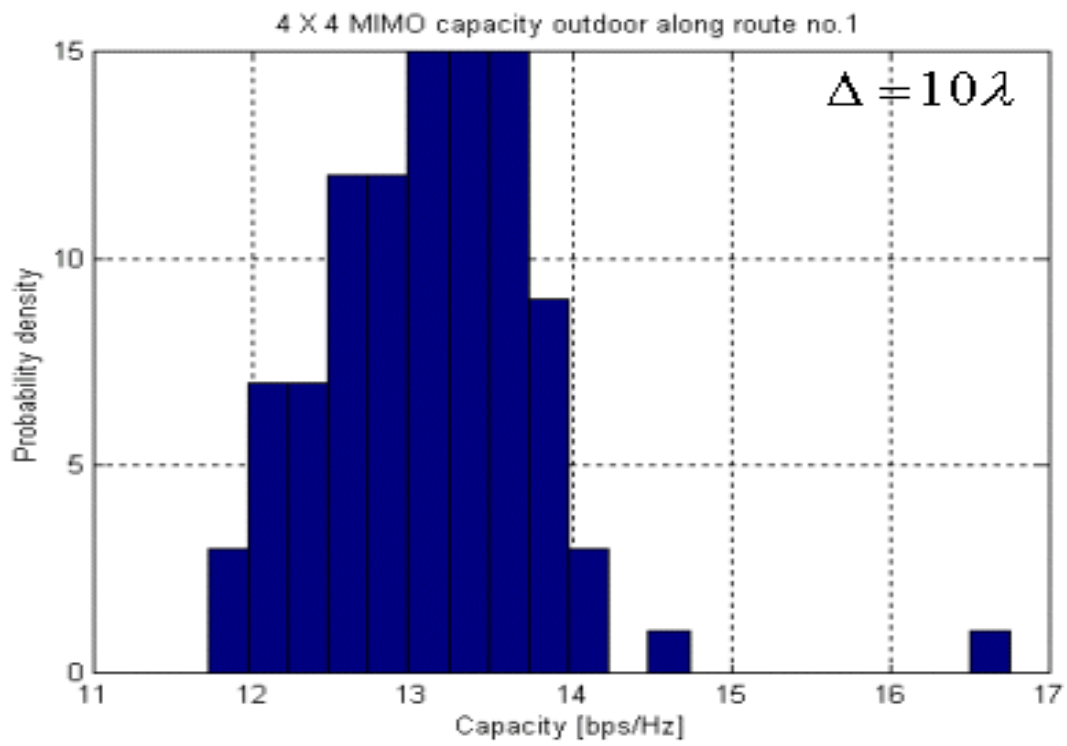
Fig 4-16 (a)
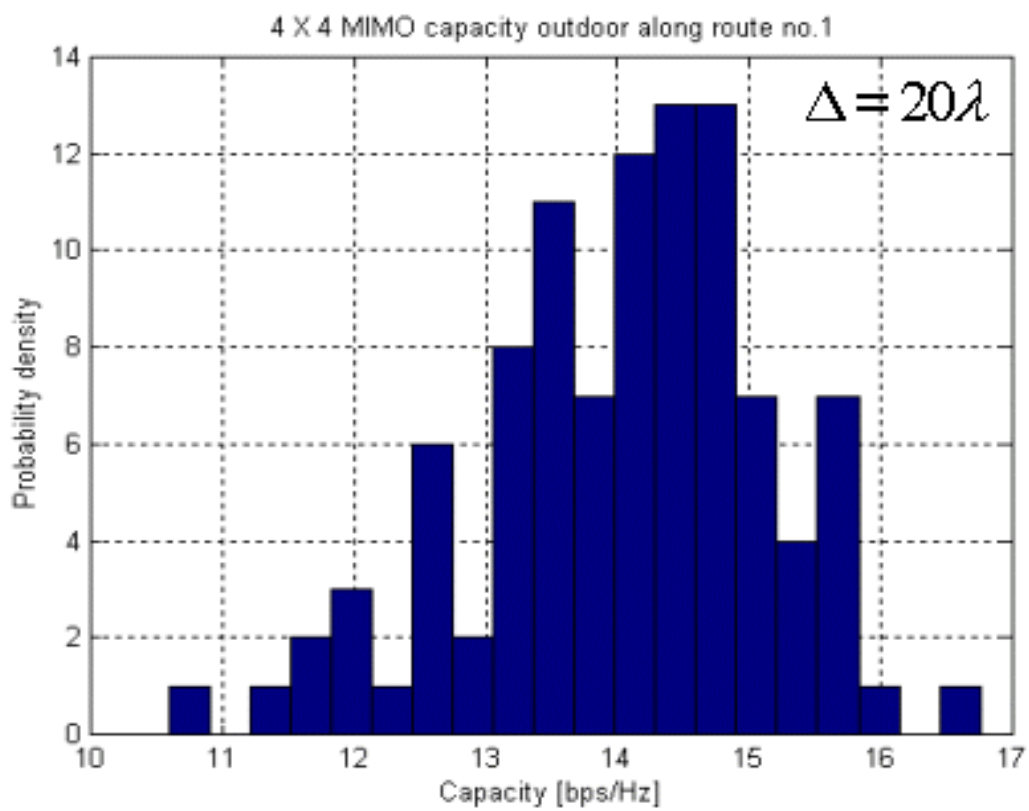
Fig 4-16 (b)
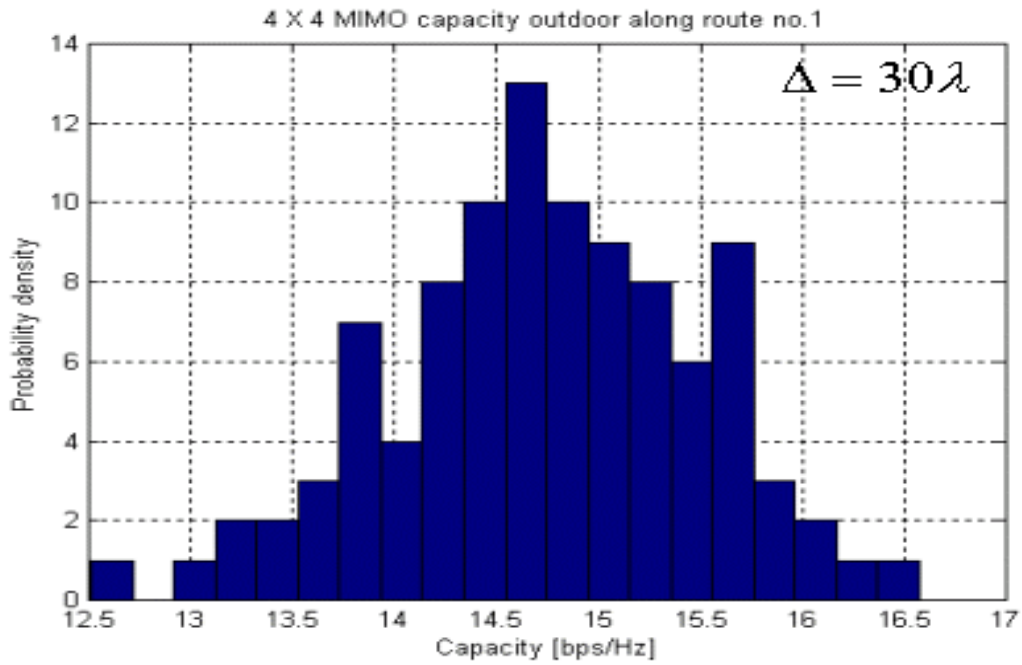
Fig 4-16 (c)

Fig 4-16 histogram corresponding to MIMO capacity for LOS along route no.1 with
(a) $\Delta = 10\lambda$ (b) $\Delta = 20\lambda$ (c) $\Delta = 30\lambda$
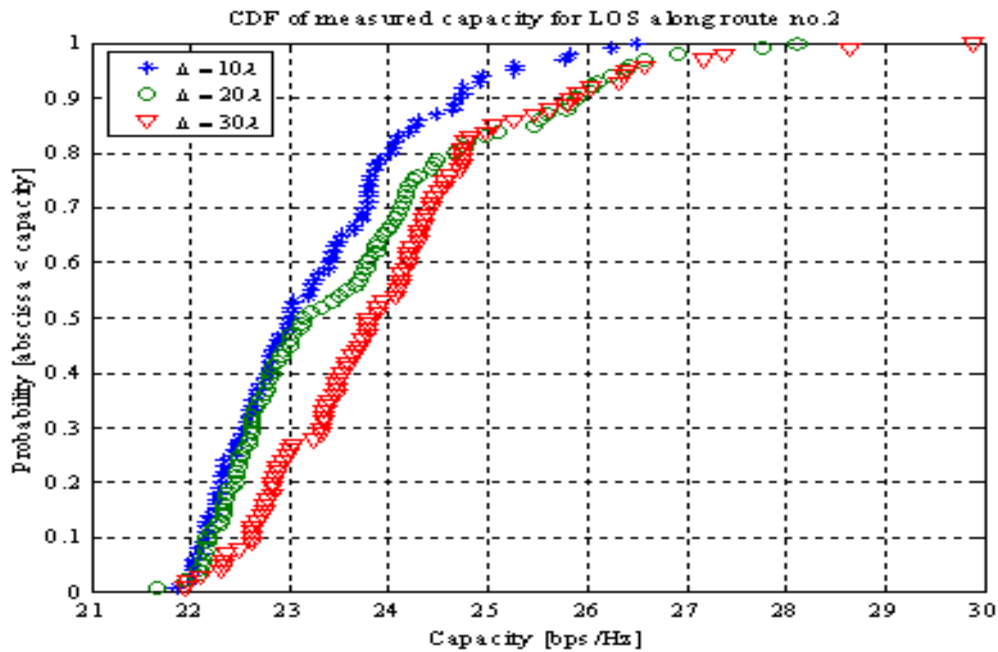
Fig 4-17 (a) The CDF of different element spacing for LOS along route no.2. The averaged capacity is 23.258 bps/Hz for $\Delta = 10\lambda$ condition, 23.6484 bps/Hz for $\Delta = 20\lambda$ condition and 24.0421 bps/Hz for $\Delta = 30\lambda$ condition.

Fig 4-17 (b) The CDF of different element spacing for LOS along route no.3. The averaged capacity is 21.7373 bps/Hz for $\Delta = 10\lambda$ condition, 22.4905 bps/Hz for $\Delta = 20\lambda$ condition and 24.0012 bps/Hz for $\Delta = 30\lambda$ condition.
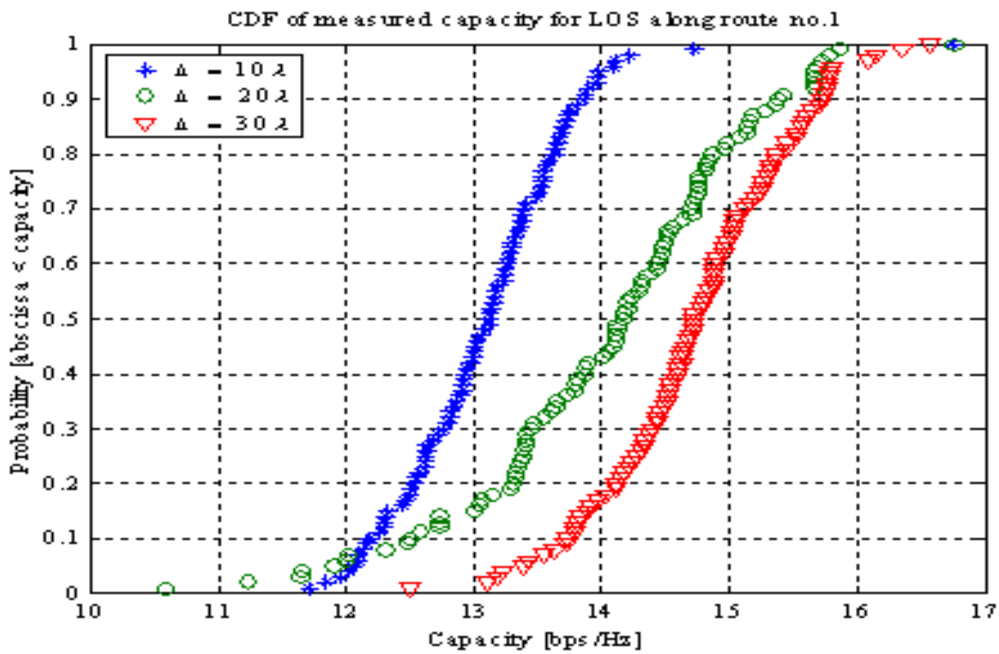

Fig 4-17 (c) The CDF of different element spacing for LOS along route no.4. The averaged capacity is 24.2358 bps/Hz for $\Delta = 10\lambda$ condition, 25.83 bps/Hz for $\Delta = 20\lambda$ condition and 26.3559 bps/Hz for $\Delta = 30\lambda$ condition.
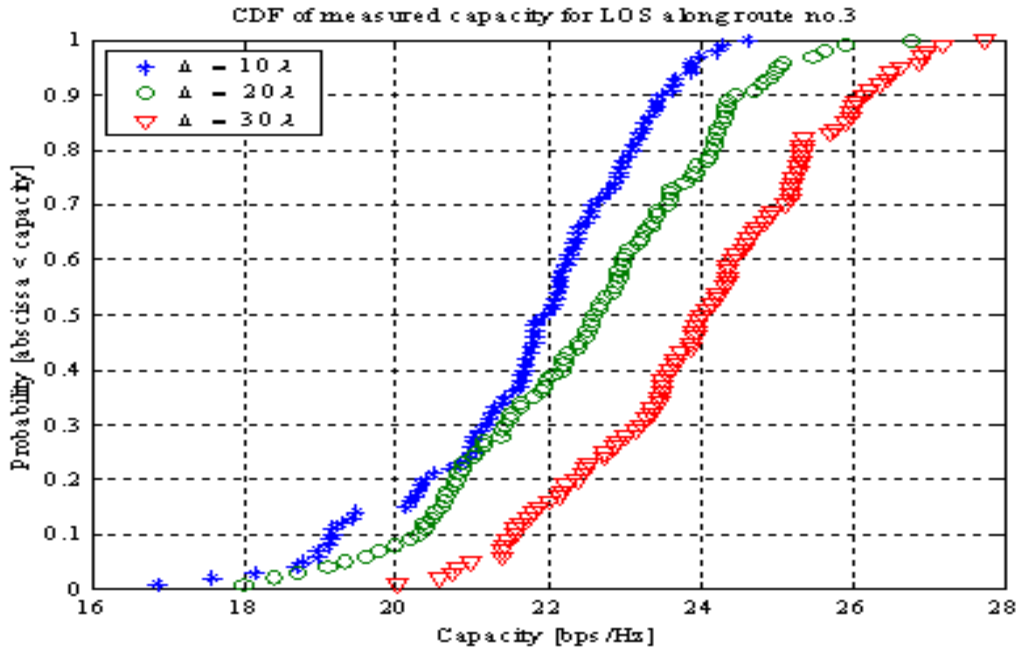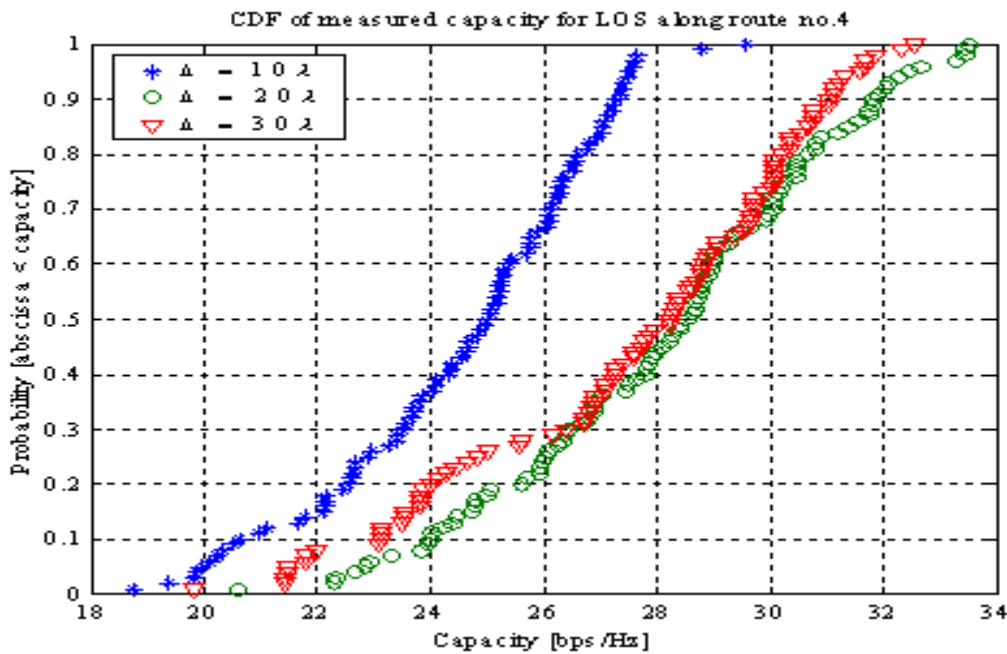
Fig 4-18 illustrates the ensemble average capacity with MIMO element spacing

of measurements. As the figure indicated, there will be a trend that capacity becomes

large as the MIMO element spacing increases for each route. Note that the values

shown in the Fig 4-18 are obtained from averaging statistically 100 times.
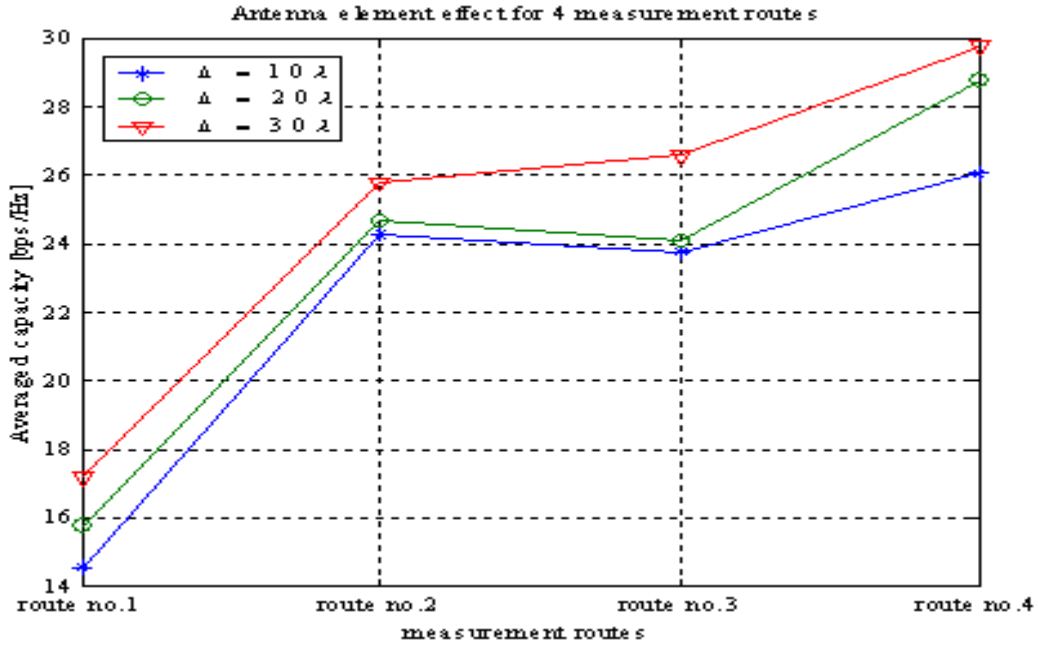
Fig 4-18 The averaged capacity with MIMO element spacing for all measurements

4.2.2 Computation with the Hybrid model

From [12], a hybrid spatio-temporal radio channel model combines a

site-specific model with a statistical model; we simulate the MIMO propagation with

different element spacing and local scatters around the transmitter, in the process of

adding the local scatters to investigate effect on MIMO capacity, there are three

categories of local scatters effect, they are the category of 3 local scatters and scatter

radius 2m with 4 different transmit element spacing 10λ, 20λ, 30λ, shown in Fig

4-19 (a); the category of scatter radius 2m and transmit element spacing 10λ with 2

to 6 local scatters, shown in Fig 4-19 (b); the category of 3 local scatters and transmit

element spacing 10λ with 3 different scatter radius 2m, 3m, 4m, shown in Fig 4-19

(c). In Fig. 4-19 (a), we note that the ensemble capacity will increase as the element

spacing increases since the array aperture is approximately M x d_t, beamwidth is

inversely proportional to aperture and resolution is inversely proportional to beamwidth, hence the larger array (d_t larger) resolves multipaths more, the propagation of MIMO channel filled with multipaths results in capacity increases. Fig 4-19 (b) and (c) present the degree of freedom of local scatter and scatter radius essentially perturb the MIMO channel and decorrelate it such that capacity distributes wider. This says the scatters within scatter radius around the transmitter will have impact on the MIMO capacity with 13.35% variation.

CDF of capacity applying the hybrid model for 3 element spacing

Fig 4-19 (a)

CDF of 6 propagation with Rs=2m
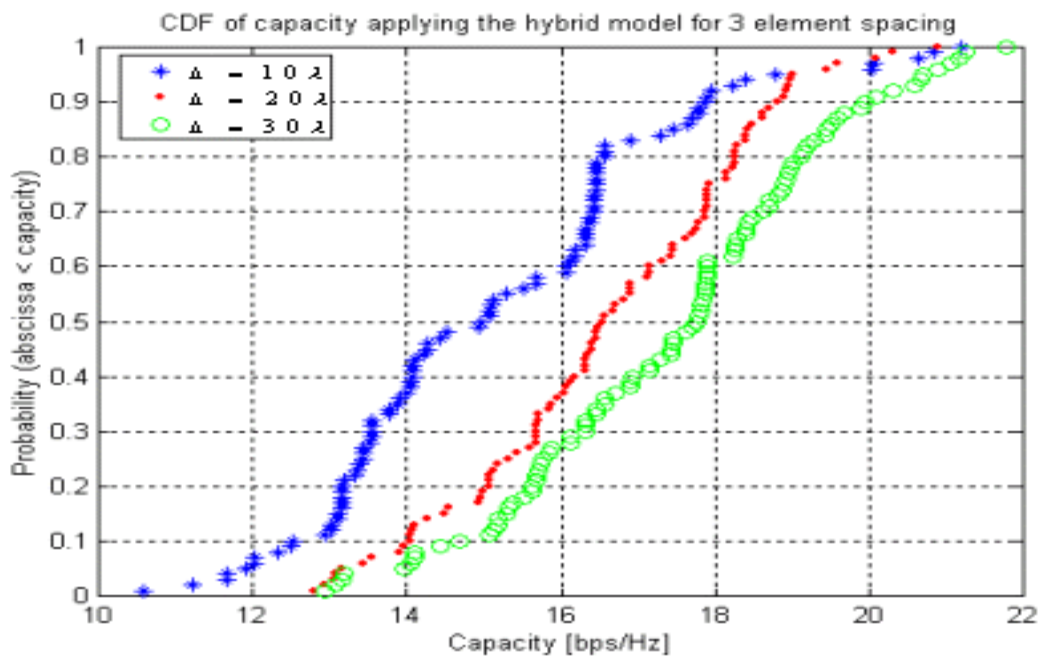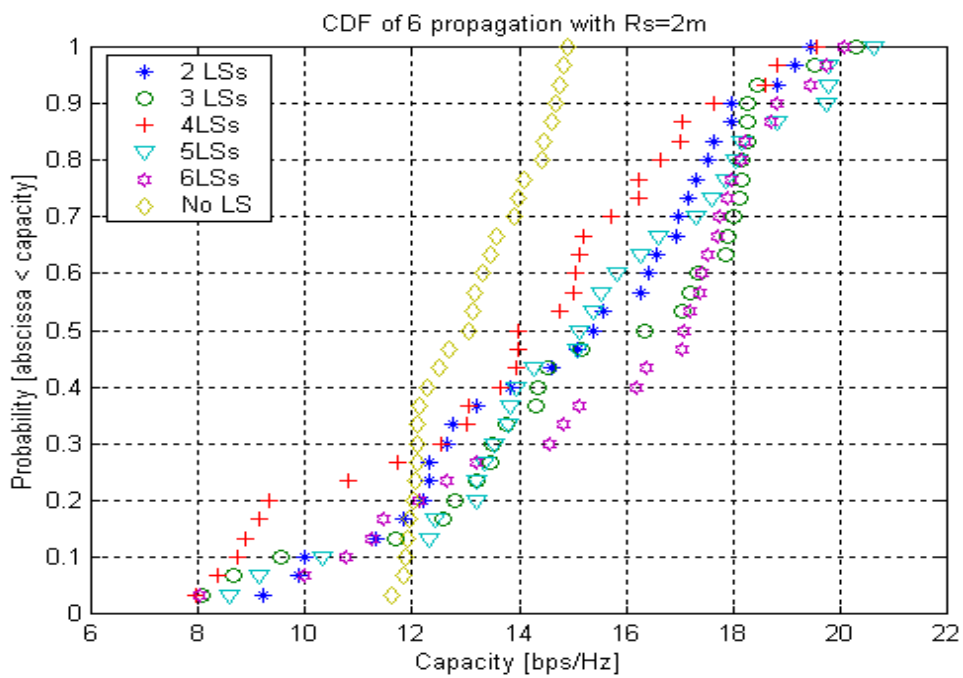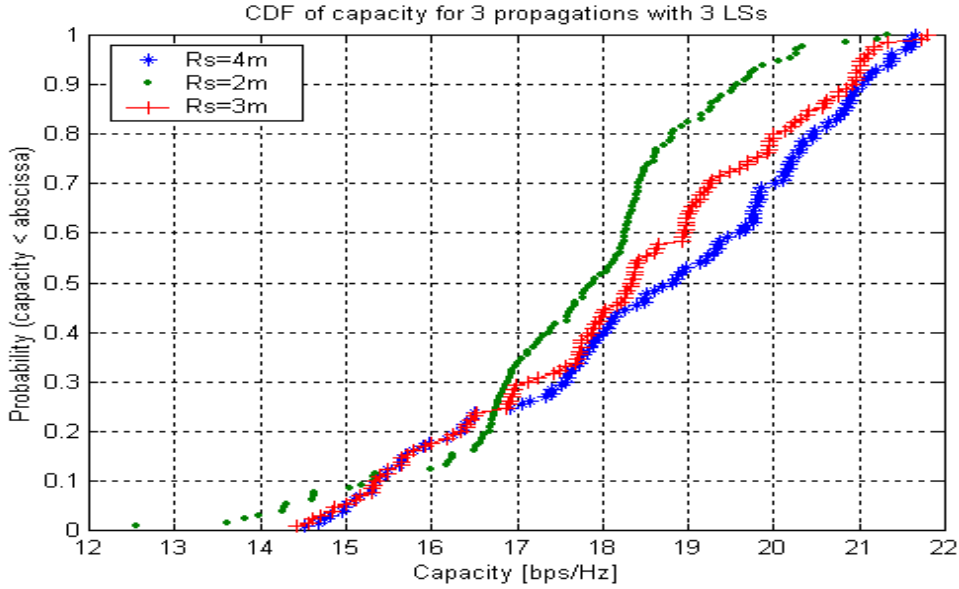
Fig 4-19 (b)

Fig 4-19 (c)

Fig.4-19 (a) CDF of capacity applying hybrid model for different element spacing. The averaged capacity is 15.1589 bps/Hz for $\Delta = 10\lambda$ condition, 16.6232 bps/Hz for $\Delta = 20\lambda$ condition and 17.4488 bps/Hz for $\Delta = 30\lambda$ condition. (b) CDF of capacity between 6 propagation under the condition of scatter radius 2m and different number of local scatterers and propagation without considering local scatter. (c) CDF of capacity for different scatterer radius

The scatter effect illustrated in the figure 4-19 (b) and (c), the simulation applying hybrid model, is obvious, we realize the sources of scatterers in the real environment not only confined with the wall effect but also the pedestrians, trees, vehicles…etc, hence the environment issues of propagation will have great impact on capacity. Next we will illustrate the CDF of capacity of measurement and hybrid model more clearly to investigate the variation of capacity due to propagation for 4 sites.

4.2.3 Comparison

From [6], given an ensemble of matrices generated by considering the density of scatters, the distribution of channel matrices is primarily a function of the number transmit and receive antennas and the density of scatters in units of $\frac{1}{d_t^2}$, where d is

the element spacing of arrays. At some large distance R~$d_{t,m}$, the contribution of a

scatters to an entry in the channel matrix is attenuated by the inverse of the distance

squared $\dfrac{1}{R^2}$. The number scatters in a differential annulus increase linearly with

distance, but the effects of the scatters combine incoherently so that the contribution

grows slowly than R and the integrated contribution from radius R to ∞ is finite.

Fig.4-20 (a)~(d) provide the comparison of CDF of capacity of different element

spacing between the measurement and hybrid model for route no.1, route no.2, route

no.3 and route no.4, respectively. For route no.1 to route no.4, we consider the

measured capacity of three kinds of element spacing in LOS propagation and applying

hybrid model taken three kinds of element spacing into account. The ensemble

average of the CDF of capacity for each element spacing does not differ from the one

applying hybrid model significantly; but there is still a trend existed that the ensemble

average of capacity of 30λ is the largest among three kinds of element spacing for

each propagation of routes; Since aperture of array becomes larger, the beamwidth

tapered increasingly therefore the resolution improves so the larger array i.e., larger

element spacing, the resolved multipaths more to obtain higher capacity. From these

four figures, the curves of the hybrid model can probably fit that of the measurement

due to the local scatters added. Hence, we can conclude that the existence of local

scatters around the transmit end array will affect the capacity performance again

although its capability is limited stated from [6].

To this end, we tabulate the mean capacity of different element spacing of each
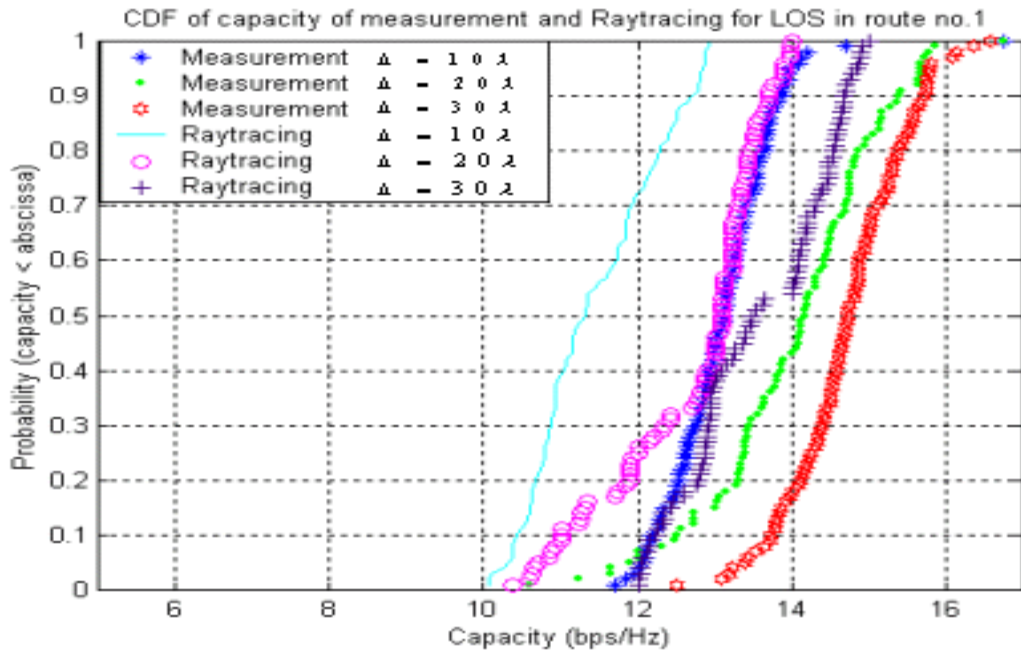
propagation for all routes as table-2.
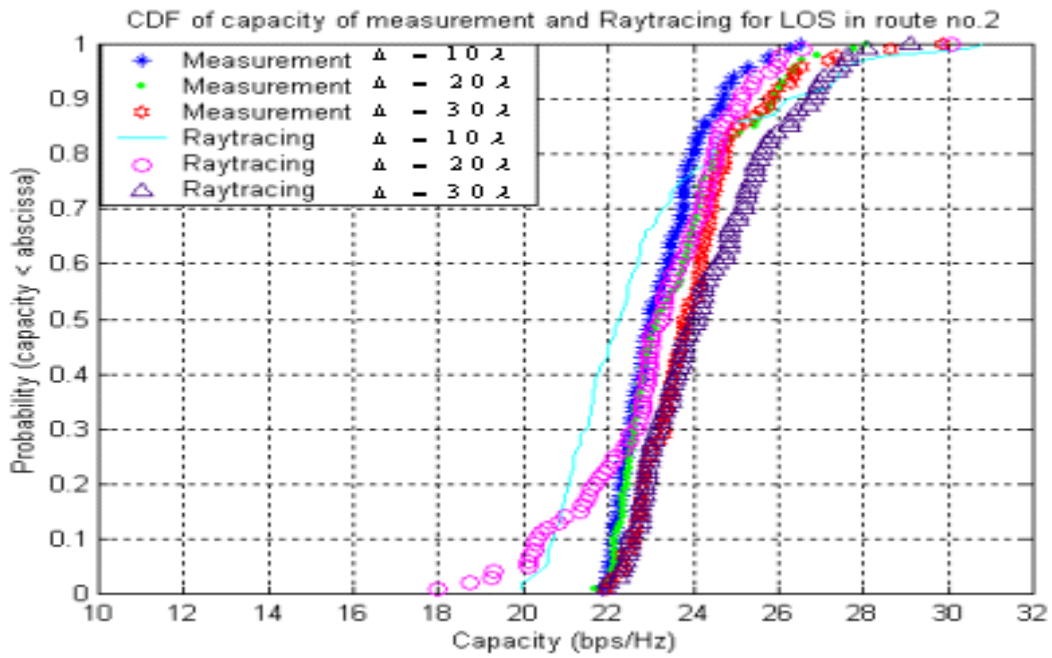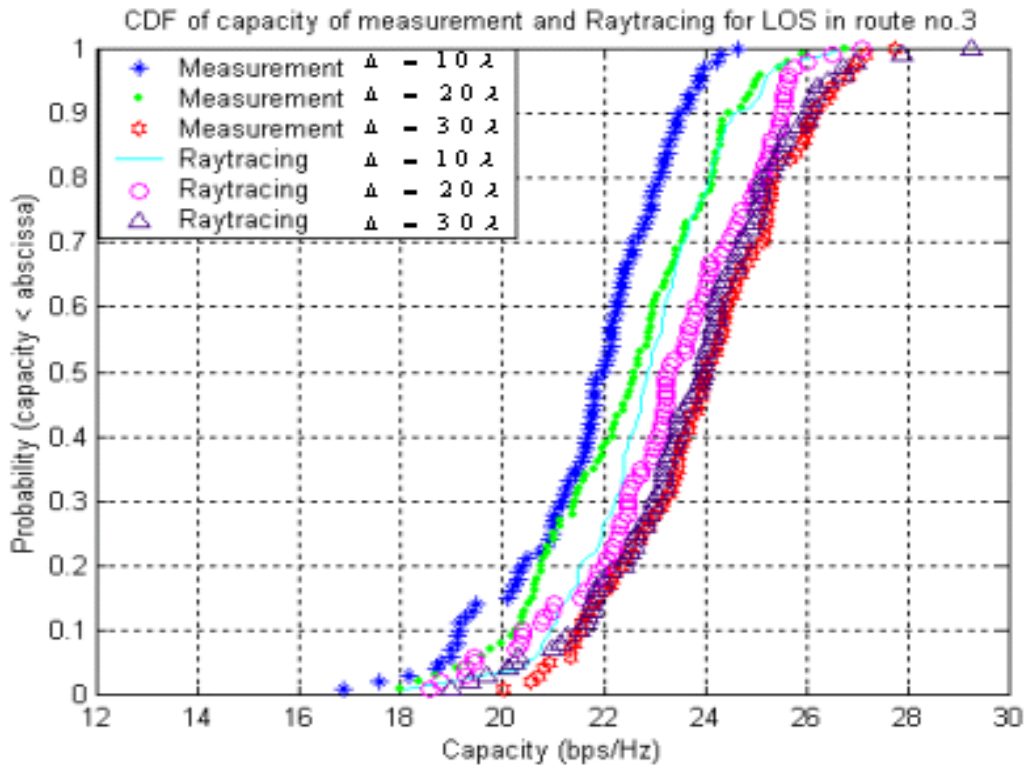
Fig 4-20 (a)
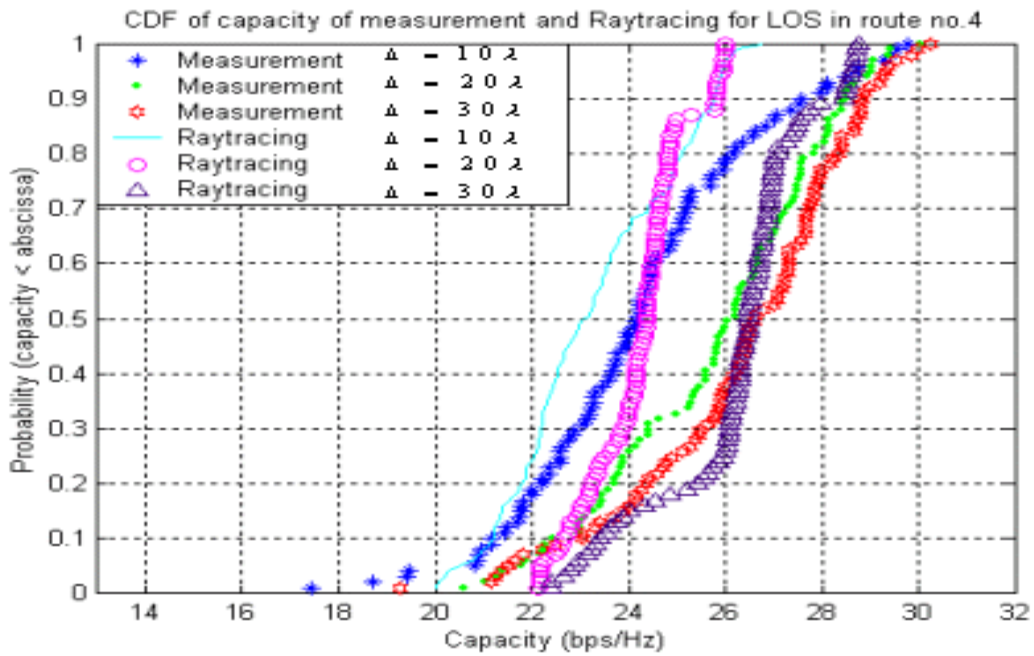

Fig 4-20 (b)

Fig 4-20 (c)

Fig 4-20 (d)

Fig 4-20 The comparison of CDF of capacity of different element spacing between the measurement and hybrid model for (a) route no.1, (b) route no.2, (c) route no.3 and (d) route no.4, respectively.

Table 2-Mean capacity [bps/Hz] for three propagation, which has three kinds of element spacing of 4 routes

Routes		Route no.1	Route no.2	Route no.3	Route no.4
LOS	10λ	13.1102	23.258	21.7373	24.2358
	20λ	14.0515	23.6484	22.4905	25.8312
	30λ	14.7372	24.0421	24.0124	26.3559
OLOS	10λ	14.9382	24.623	23.8253	25.8532
	20λ	16.6158	25.2158	24.8374	29.0958
	30λ	17.7987	25.6486	27.7044	30.6944
NLOS	10λ	15.65	24.6787	25.732	27.6917
	20λ	17.6539	26.5171	26.1283	30.0702
	30λ	18.9749	27.6596	27.9885	31.0142

4.3.1 Bandwidth Effect

A. Along route no.1 (LOS-OLOS-NLOS)

For measurement of routes, we make a table to record the mean capacity, standard deviation of capacity, standard deviation of rms azimuth spread of AOA and standard deviation of rms azimuth spread of AOD shown as Table-3. From this table we consider the bandwidth effect on the capacity. Fig 4-21 illustrates the capacity versus signal bandwidths. It is found that the capacity increases as the signal bandwidth increases for the LOS, OLOS or NLOS propagation situation along route no.1. It is because that as bandwidth becomes large, time resolution decreases [14]; hence array resolved more multipaths perturbed the signal correlation between transmitter and receiver. Figs 4-22 presents the maximum, minimum and mean values for each propagation of different bandwidth of routes. Similar results of MIMO capacity versus signal bandwidths can be found in the figures 4-23, 4-24 and 4-25 to stand for route no.2, route no.3 and route no.4, respectively.

Fig 4-21 The capacity versus signal bandwidths for three propagation conditions LOS, OLOS and NLOS along route no.1

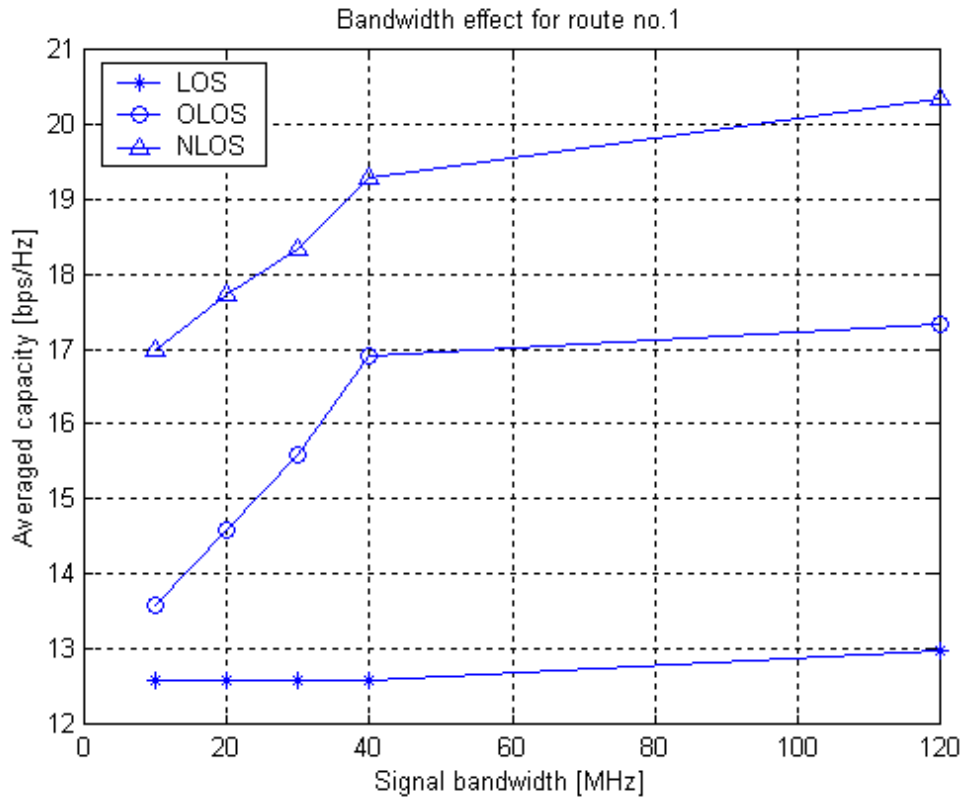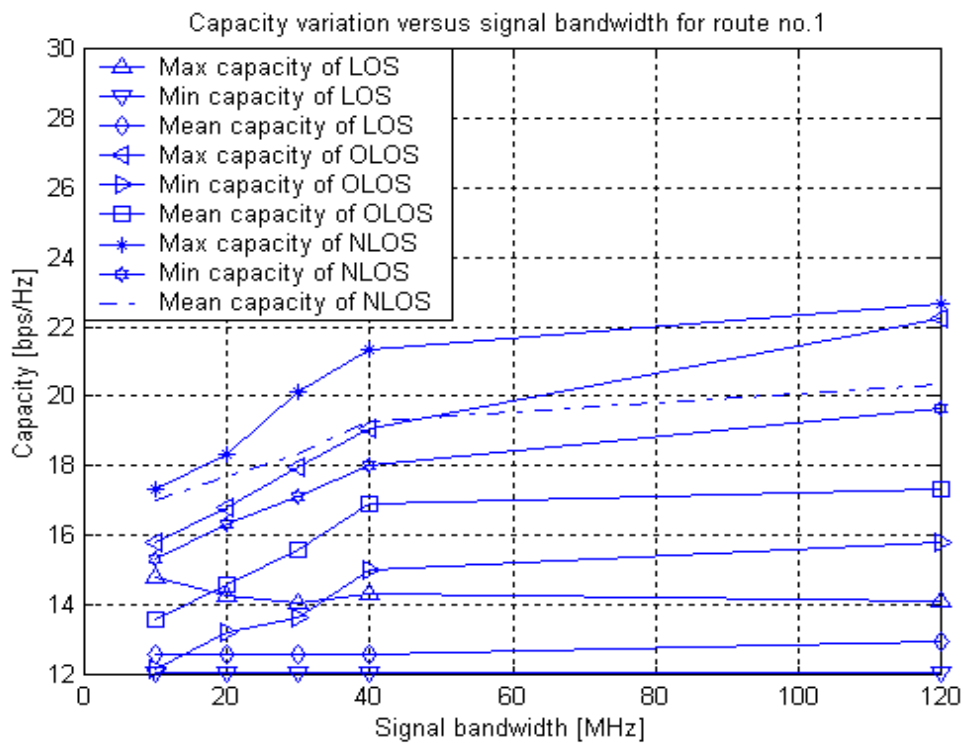Figs 4-22 The maximum, minimum and mean values for three propagation conditions LOS, OLOS and NLOS of different bandwidth along route no.1
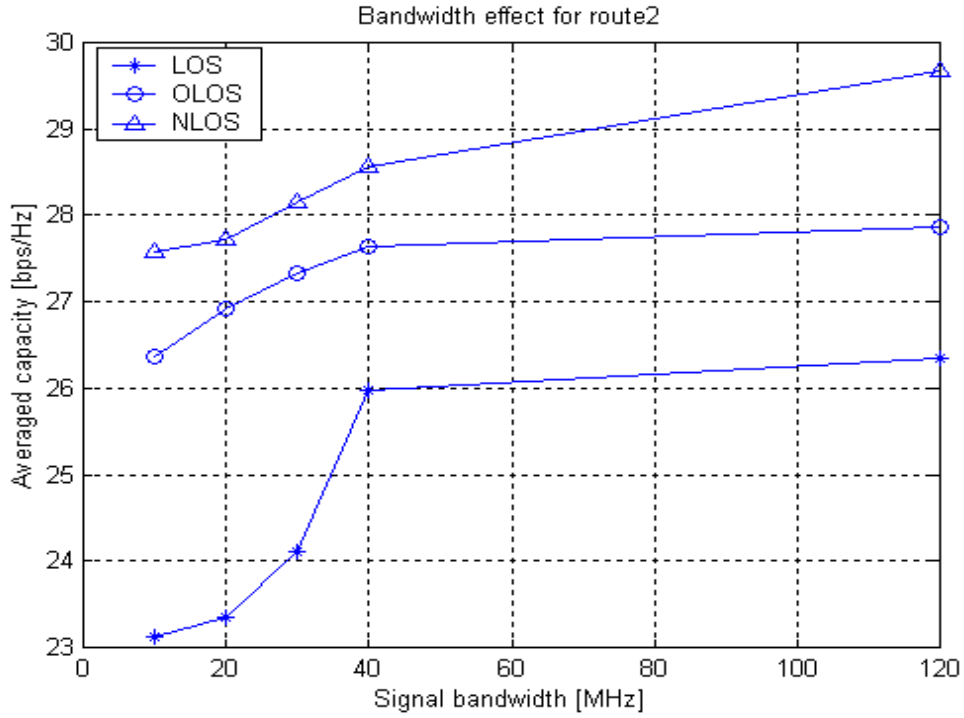
Fig 4-23 The capacity versus signal bandwidths for three propagation conditions LOS, OLOS and NLOS along route no.1
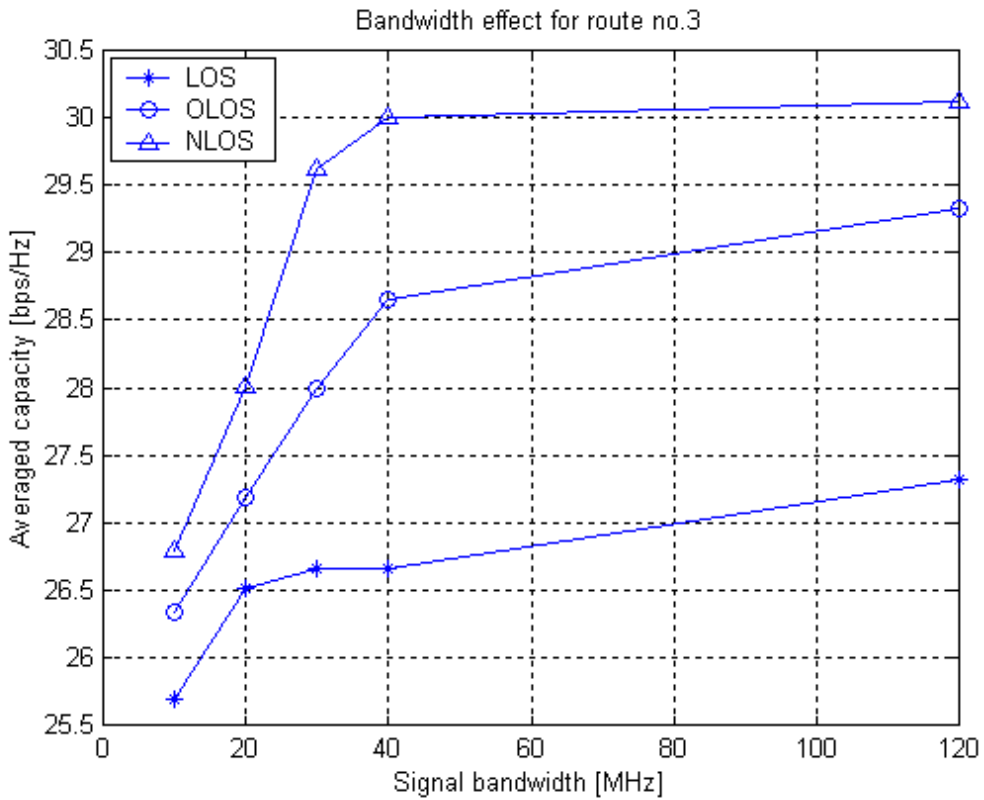
Fig 4-24 The capacity versus signal bandwidths for three propagation conditions LOS, OLOS and NLOS along route no.3.
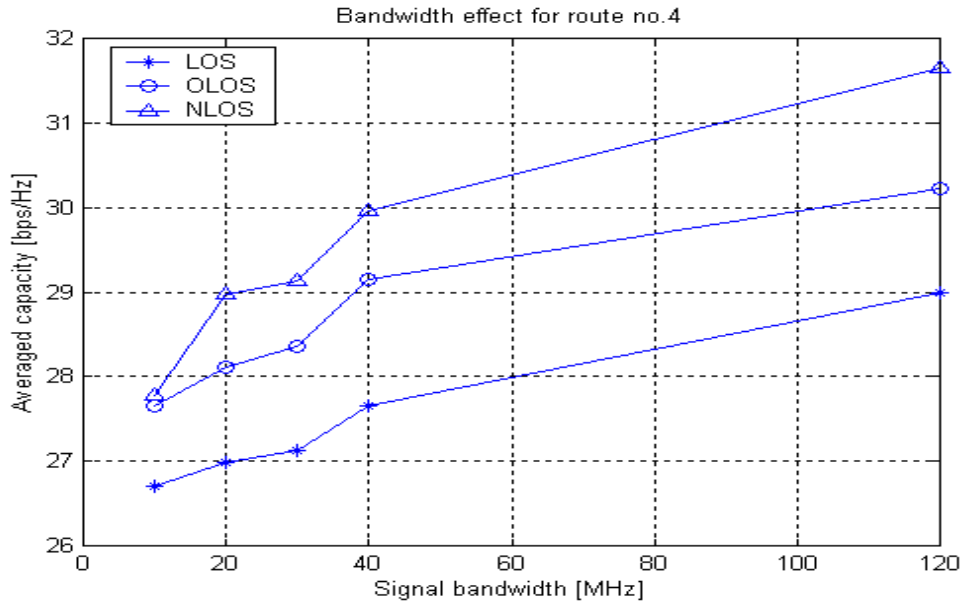
Fig 4-25 The capacity versus signal bandwidths for three propagation conditions LOS, OLOS and NLOS along route no.4.

4.3.2 Angle Spread Effect

From Table-3 we realize the fact that capacity and azimuth spread of AOA present a positive correlation shown as Fig 4-23, but indifferent with azimuth spread of AOD. Azimuth spread of AOA means the angle dispersion caused by multipaths propagating in the channel owing to ground reflection wave, corner diffracted wave, scattered wave…etc. These mulitpaths can disturb the propagation channel of signals resulting in the transmitted signal received by array less correlated, even uncorrelated. But angular spread of AOD means the angular dispersionness from transmitter; it does not yet propagate through MIMO channel to interference the capacity, hence the azimuth spread of AOD does not present obvious correlation with capacity. The condition hold for site2, site3 and site4, we note that the capacity of LOS in site1 is smaller than that of site2, site3 and site4, since scatters existed in the environment and site1 is LOS with open-area, short distance but for the site2, site3 and site4 cases, we can resolve the scattered wave in terms of time resolution and azimuth resolution to

observe how the channel interfered by the scatters shown Fig 4-24. Figure 4-24 provides the Delay-Azimuth Spectrum of measurement data and the resolved scattered wave (*) on the time and azimuth resolution and CDF of capacity for subchannels and eigenvalue distribution of measurement for site2 (a), site3 (b) and site4 (c) since we have realized the impact of propagation on capacity. While we compute the number of scatter waves, an assumption of single bounce is made. From the number resolved, Site2-28, Site3-59, Site4-89, we realize the scattered waves impinged on transmitter more, the propagation channel decorrelated more, hence the capacity will have a significant improvement.

Table-3 the mean capacity, standard deviation of capacity, standard deviation of rms of azimuth spread of AOA and standard deviation of rms of azimuth spread of AOD for all measurement sites.

Site1		Mean Capacity (bps/Hz)	Standard deviation of capacity (bps/Hz)	Mean Azimuth spread of AOA (degree)	Mean Azimuth spread of AOD (degree)
LOS	10MHz	12.5744	0.5742	2.1451	5.7567
	20MHz	12.5746	0.5572	2.511	5.5249
	30MHz	12.5795	0.5394	2.3251	5.6978
	40MHz	12.5891	0.5238	2.2441	5.5375
	120MHz	12.9648	0.5112	2.654	5.8422
OLOS	10MHz	13.589	2.7712	15.8041	6.9648
	20MHz	14.5971	2.3862	16.828	8.7803
	30MHz	15.601	1.9994	17.9906	8.3856
	40MHz	16.9116	1.8949	19.0632	5.0975
	120MHz	17.3351	1.6635	22.2364	4.652
NLOS	10MHz	16.9925	1.9356	31.179	6.1247
	20MHz	17.7187	1.8579	32.1872	6.0682
	30MHz	18.327	1.6653	32.915	8.4886
	40MHz	19.2765	1.4237	33.0975	7.8716
	120MHz	20.3394	1.2148	34.6584	6.354

Site2		Mean Capacity (bps/Hz)	Standard deviation of capacity (bps/Hz)	Mean Azimuth spread of AOA (degree)	Mean Azimuth spread of AOD (degree)
LOS	10MHz	23.1249	2.9949	1.1249	12.325
	20MHz	23.3548	2.8486	1.3165	12.1248
	30MHz	24.1073	2.6603	1.9132	13.1984
	40MHz	25.9841	2.2124	2.321	13.442
	120MHz	26.3549	1.6698	2.654	14.228
OLOS	10MHz	26.3741	3.2526	6.2256	17.0993
	20MHz	26.9251	3.0239	6.5965	16.1107
	30MHz	27.3275	2.9305	7.5699	17.9916
	40MHz	27.6367	2.8826	7.9134	16.1296
	120MHz	27.8621	2.1156	8.6632	16.2654
NLOS	10MHz	27.5714	2.8826	21.4134	17.4513
	20MHz	27.7262	2.5237	22.0648	19.2507
	30MHz	28.1597	2.2319	22.5965	17.0461
	40MHz	28.5594	2.0655	23.5801	18.6209
	120MHz	29.6654	1.9354	24.3215	16.3324

Site3					
		Mean Capacity (bps/Hz)	Standard deviation of capacity (bps/Hz)	Mean Azimuth spread of AOA (degree)	Mean Azimuth spread of AOD (degree)
LOS	10MHz	25.6859	2.8282	3.2395	5.3188
	20MHz	26.5091	2.6831	4.1735	5.2126
	30MHz	26.6621	2.3399	4.9934	9.1876
	40MHz	26.6632	1.9483	5.0935	4.6711
	120MHz	27.325	1.5984	5.1654	4.3258
OLOS	10MHz	26.3354	2.3542	12.2238	15.648
	20MHz	27.1849	1.8421	12.9842	15.6248
	30MHz	27.9984	1.6548	13.201	18.6549
	40MHz	28.6548	1.3315	14.6548	15.2203
	120MHz	29.3326	0.9652	15.654	15.328
NLOS	10MHz	26.7864	1.9543	28.7892	29.3845
	20MHz	28.0015	1.7749	29.3514	25.3259
	30MHz	29.6259	1.5563	29.9658	25.3695
	40MHz	29.9953	1.2684	30.1841	26.1248
	120MHz	30.1124	1.1651	32.3248	25.324

| Site4					
		Mean Capacity (bps/Hz)	Standard deviation of capacity (bps/Hz)	Mean azimuth spread of AOA (degree)	Mean Azimuth spread of AOD (degree)
LOS	10MHz	26.7055	1.2078	5.0205	13.0595
	20MHz	26.9923	1.1938	5.2461	12.2567
	30MHz	27.1198	1.1424	5.9244	12.1993
	40MHz	27.6459	1.1104	6.7018	13.6646
	120MHz	28.9986	1.0358	7.1268	13.326
OLOS	10MHz	27.6544	2.9354	12.6648	23.2698
	20MHz	28.1168	2.6328	16.6528	23.2268
	30MHz	28.3546	2.4562	19.948	23.4485
	40MHz	29.1436	1.9845	21.9946	23.7246
	120MHz	30.2264	1.5264	24.226	23.228
NLOS	10MHz	27.7715	1.9324	34.235	6.1496
	20MHz	28.9684	1.7653	34.984	6.1359
	30MHz	29.1256	1.5945	35.1458	6.335
	40MHz	29.9564	1.4652	35.3359	7.6523
	120MHz	31.6542	1.3s325	36.2268	7.321
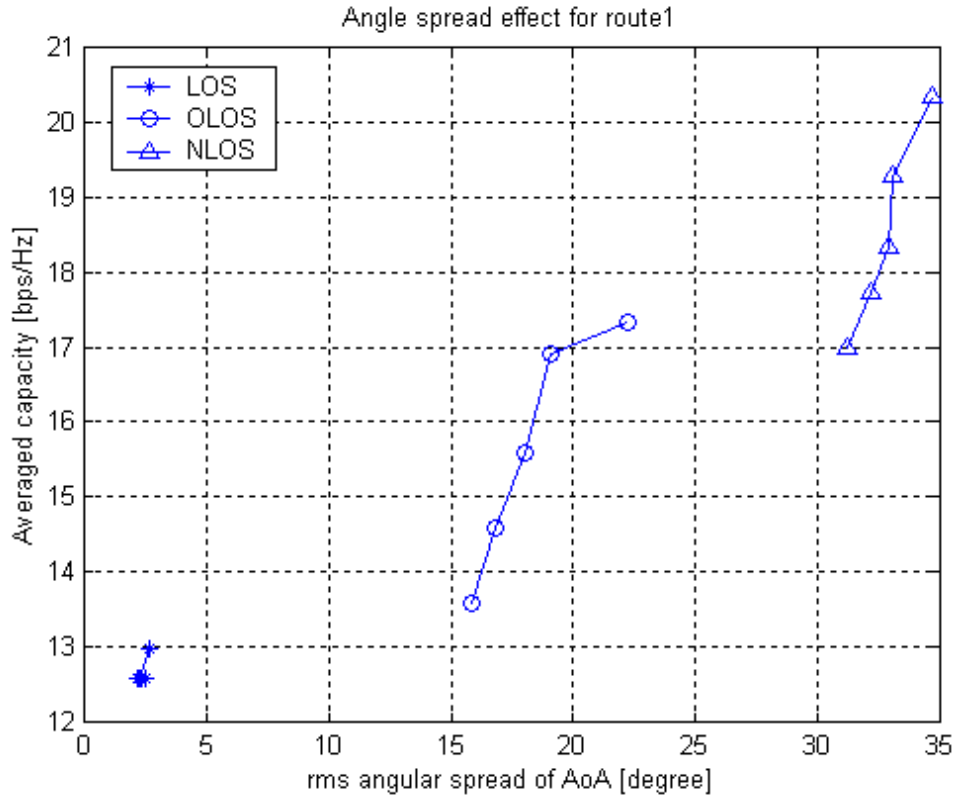
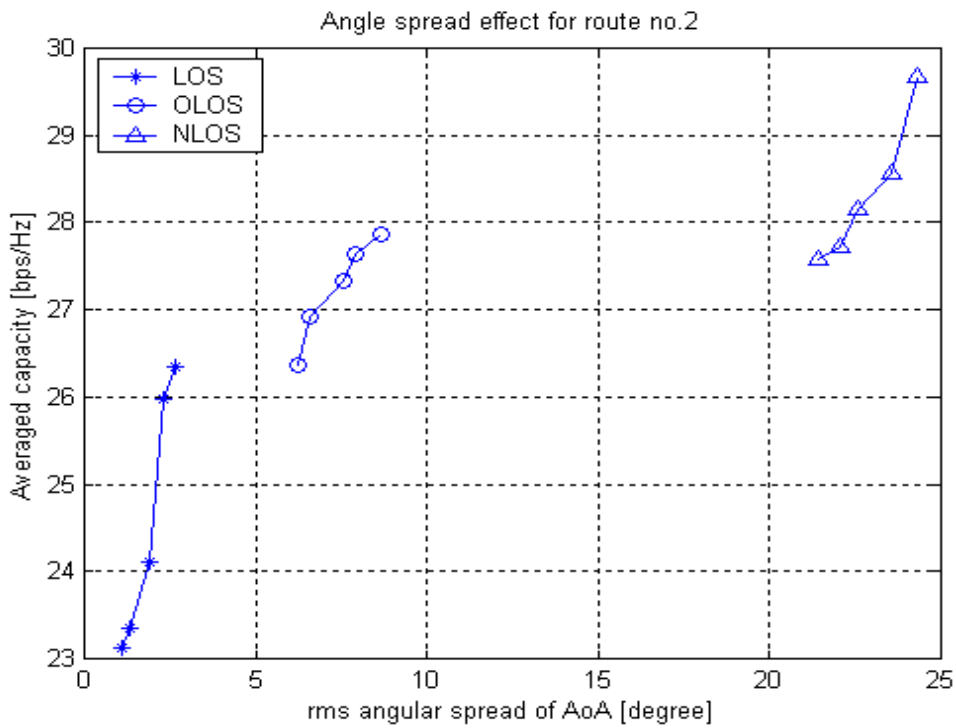Fig 4-26 (a) capacity versus rms azimuth spread of AOA for route no.1

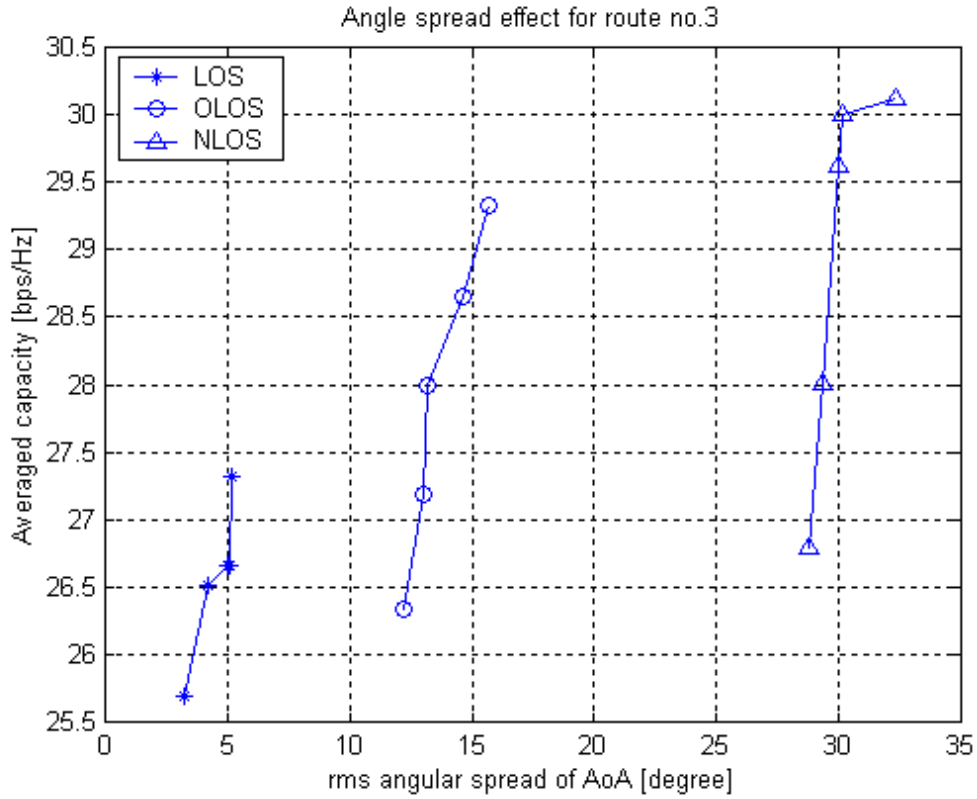Fig 4-26 (b) capacity versus rms azimuth spread of AOA for route no.2

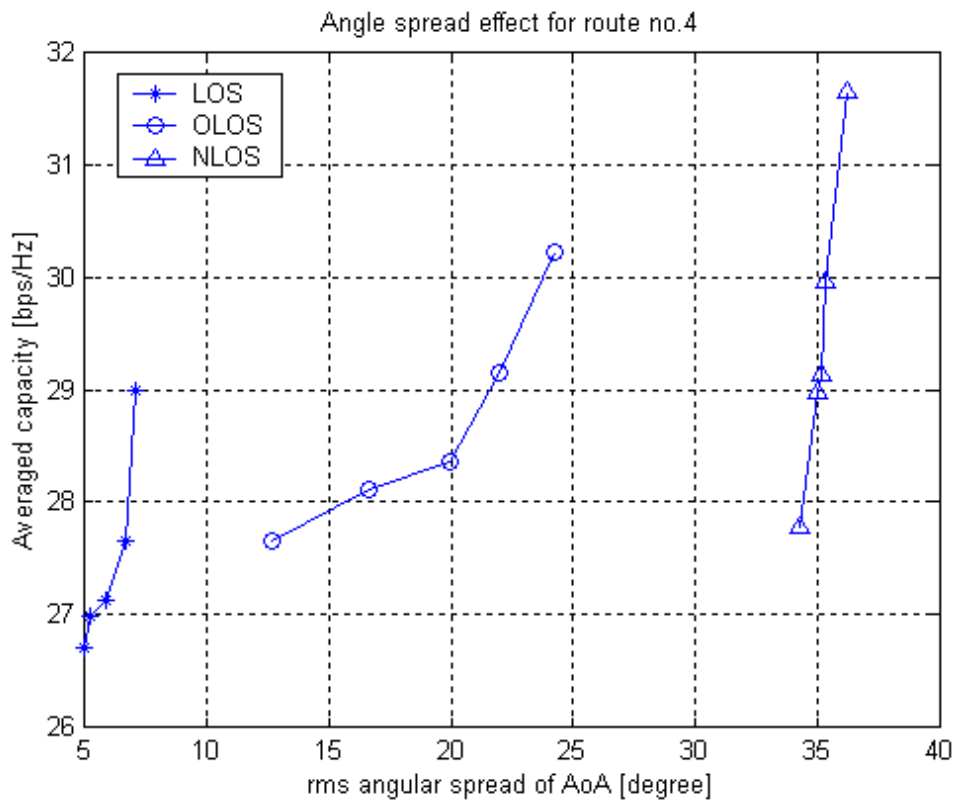Fig 4-26 (c) capacity versus rms azimuth spread of AOA for route no.3

Fig 4-26 (d) capacity versus rms azimuth spread of AOA for route no.4

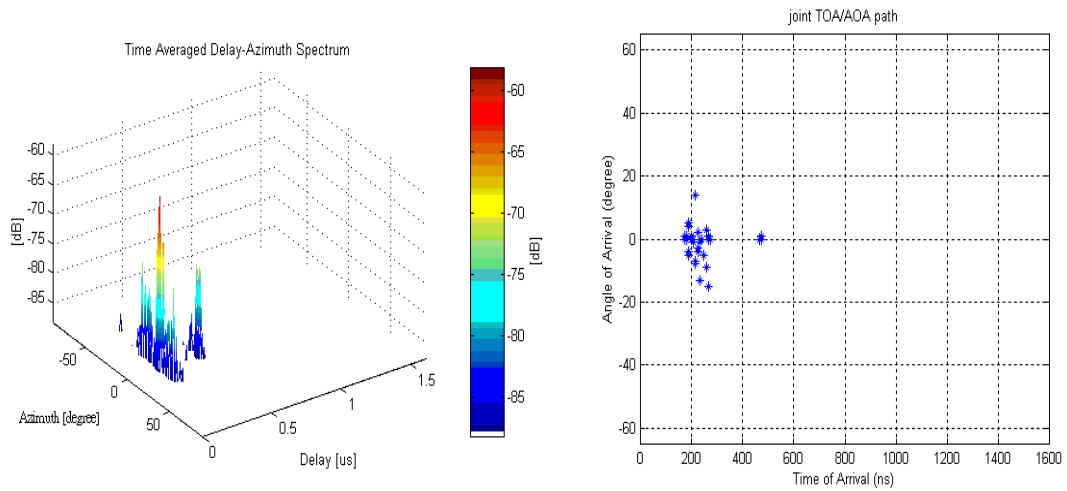Time Averaged Delay-Azimuth Spectrum

joint TOA/AOA path

Corresponding capacity of per channel & eigenvalue distribuiotn

Fig 4-27 (a)

Time Averaged Delay-Azimuth Spectrum

joint TOA/AOA path

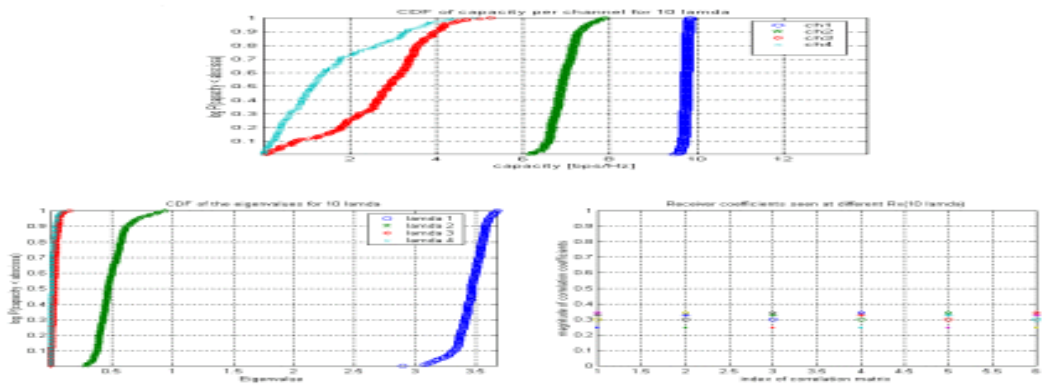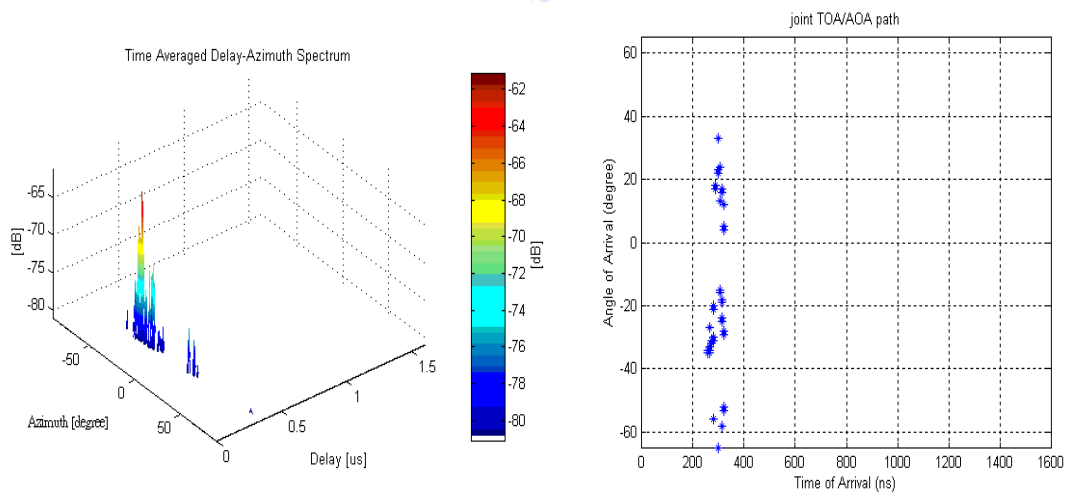## Corresponding capacity of perchannel & eigenvalue distribution
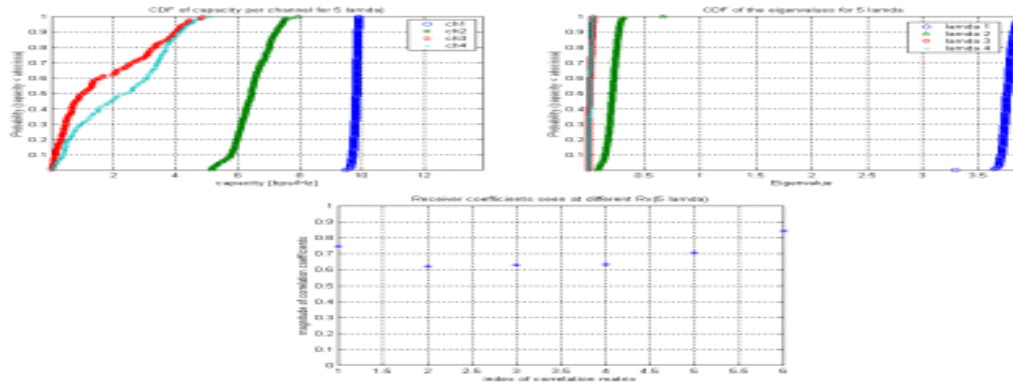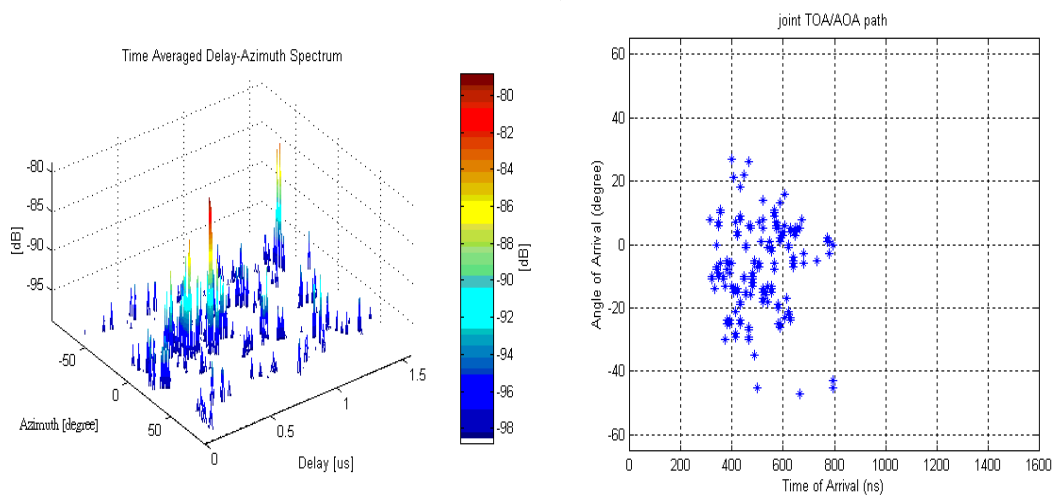

Fig 4-27 (b)

Corresponding capacity of per channel & eigenvalue distribuiotn

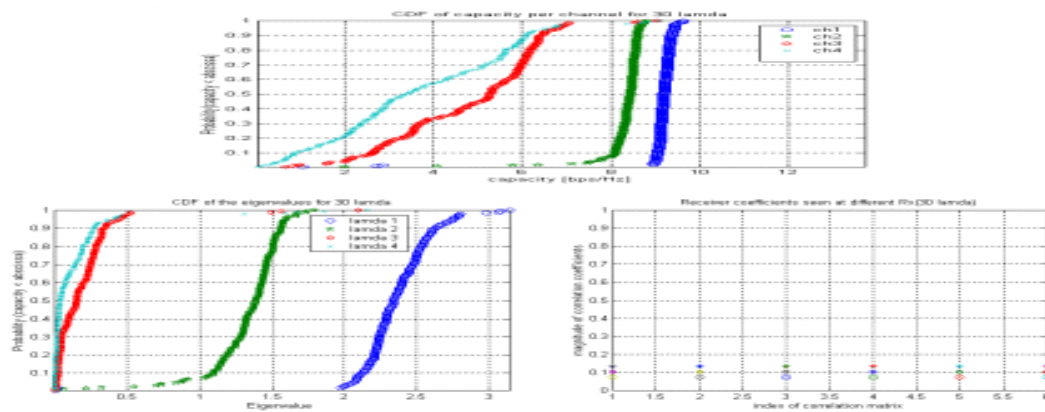
Fig 4-27 (c)

Figure 4-27 the Delay-Azimuth Spectrum of measurement data and the resolved scattered wave (*) on the time and azimuth resolution and CDF of capacity for subchannels and eigenvalue distribution of measurement for (a) route no.2 (b) route no.3 and (c) route no.4.

Chapter 5

Conclusion

In this thesis the analysis of the effect of propagation and antenna arrangement on 4X4 MIMO capacity has been presented. Three propagation conditions such as LOS, OLOS and NLOS are considered. Furthermore, effects due to propagation distance, bandwidth and angular spread are also considered. The measurement using the RUSK channel sounder was carried in the National Chiao-Tung University campus.

As far as propagation conditions are concerned, the capacity in the NLOS condition ensures a high probability to be larger than the LOS and OLOS conditions due to larger angular dispersion. As for MIMO system with the same element spacing located at different routes, capacity increases due to transmitted signals disturbed by the local scatter so that the spatial correlation of receiving signals decreases. Environment must be complex enough to disturb the spatial correlation of receiving signals so that capacity becomes larger.

For the different element spacing effect, capacity of MIMO system under particular site increases due to the resolution of multipaths seen from the receive end array increases. From hybrid model, we know that local scatters surrounded by the transmit end array will cause large capacity fluctuation.

For the bandwidth effect, MIMO capacity will increase as the signal bandwidth increases. This phenomenon is hold for each route under this measurement.

For the rms angular spread of AOA effect, MIMO capacity increases as the rms

angular spread of AOA increases since the multipaths propagated within larger rms angular spread of AOA probably experienced complex channel so that disturb the spatial correlation of signals. Finally, we evaluate the complexity of the channel influenced by local scatters using the number of resolved scatter waves based on temporal and angular resolution.

References

[1] G. J. Foschini and M. J. Gans, "*On limits of Wireless Communications in a Fading Environment When Using Multiple Antennas*," *Wireless Personal Communications*, vol. 6, No. 3, pp. 311-335, March 1998

[2] A. Lozano, F. R. Farrokhl and R. A. Valenzuela, "*Lifting the Limits on High-Speed Wireless Data Access Using Antenna Arrays*," IEEE Communications Magazine, pp. 156-162, September 2001.

[3] Jean Philippe Kermoal, Preben E. Mogensen, Soren HH. Jensen, Jorgen B. Andersen, Frank Frederiksen, Troels B. Sorensen and Klaus I. Pedersen, "§Experimental Investigation of Multipath Richness for Multi-Element Transmit and Receive Antenna Arrays", IEEE Vehicular Technology Conference VTC 2000 Spring, Tokyo, Japan, vol.3, pp. 2004-2008, May 2000

[4] Da-shan Shiu, Gerard J. Foschini, Michael J. Gans and Joseph M. Kahn, "§Fading Correlation and Its Effect on the Capacity of Multielement Antenna Systems", IEEE Transactions on Communications, vol. 48, no.3, pp. 502-513 March 2000.

[5] Daniel W. Bliss, Keith W. Forsythe, Alfred O. Hero and Ali F. Yegulalp, "§Environment Issues for MIMO Capacit", IEEE Transactions on Signal Processing, vol.50, no.9, pp.2128-2141 September 2002.

[6] D. Gesbert, H. Boleskei, D. A. Gore and A. J. Paulraj, "§Outdoor MIMO Wireless Channels-Models and Performance Prediction", IEEE Transactions on Communications, pp.1-21 Aug. 2000,

[7] Jorgen Bach Andersen, "*Array Gain and Capacity for Known Random Channels with Multiple Element Arrays at Both Ends,*" IEEE Journal on Selected Areas in Communications, vol. 18, no. 11, pp. 2171-2178, November 2000

[8] Thomas M. Cover and Joy A. Thomas, "*Elements of Information Theory*," Wiley, 1991

[9] Andreas F. Molisch, "*A generic model for MIMO wireless propagation channels," Communications, 2002. ICC 2002. IEEE International Conference on*, vol. 1, 28 April-2 May 2002 , pp. 277 –282

[10] Reiner S. Thoma, Dirk Hampicke, Andreas Richter, Gerd Sommerkorn, Axel Schneider, Uwe Trautwein and Walter Wirnitzer, "§Identification of TimeVariant Directional Mobile Radio Channels", IEEE Transactions on Instruction and Measurement, vol.49, no.2 pp.357-364 April 2000

[11] Martin Haardt, and Josef A. Nossek, "Unitary ESPRIT: How to Obtain Increased Estimation Accuracy with a Reduced Computational Burden", IEEE Transactions on Signal Processing, vol.43, no.5, pp.1232-1243 May 1995.

[12] Yu-Jiun Ren and Jenn-Hwan Tarng, "A Hybrid Spatio-Temporal Radio Channel Model for Macrocellular Environments", June 2002.

[13] R. G. Gallager, "*Information Theory and Reliable Communication*," Wiley, 1968

[14] T. S. Rappaport, "*Wireless Communications Principles and Practice*," Prentice Hall, 1996.